Simulation studies of π^0, η and ω meson reconstruction performance in pp collisions at $\sqrt{s} = 14$ TeV in Forward Calorimeter(FoCal), ALICE

SHANKAR NAIR

Master thesis

DEPARTMENT OF PHYSICS

INDIAN INSTITUTE OF TECHNOLOGY INDORE

MAY 2023

Certificate

I hereby certify that the work which is being presented in the thesis entitled **“Simulation studies of π^0, η and ω meson reconstruction performance in pp collision at $\sqrt{s} = 14$ TeV in Forward Calorimeter(FoCal), ALICE ”** in the partial fulfilment of the requirements for the award of the degree of **Master of Science** and submitted in the **Discipline of Physics, Indian Institute of Technology Indore**, is an authentic record of my own work carried out during the time period from July 2022 to June 2023 under the supervision of **Prof. Ankhi Roy, Professor, Indian Institute of Technology Indore.** The matter presented in this thesis has not been submitted by me for the award of any other degree of this or any institute.

Signature of the student with date

27 May 2023 **(Shankar Nair)**

This is to certify that the above statement made by the candidate is correct to the best of my knowledge.

28/05/2023

Signature of the Supervisor of M.Sc. thesis (with date)

(Prof. Ankhi Roy)

Acknowledgements

It is important to acknowledge the support and contributions of individuals who have played a role in one's academic journey. I would like to express my gratitude towards my parents and elder brother for their constant encouragement and support. Additionally, I am grateful to my supervisor Prof. Ankhi Roy for her guidance and motivation during my time pursuing my MSc at IIT Indore. I would also like to extend my thanks to Dr. Ionut Cristian Arsene(Univeristy of Oslo, Norway) and Dr. Mriganka Mouli Mondal(National Institute of Science Education and Research, India (NISER)) for their invaluable advice and support during my master's project. Special thanks goes to my roommate Bhuwan for engaging in stimulating physics discussions with me. I also acknowledge the help of my PhD seniors and the members of the FOCAL Physics Simulation Group for their valuable input on my work.

Abstract

This thesis primarily focuses on π^0, η and ω meson reconstruction performance in pp collision at $\sqrt{s}$ = 14 TeV in Forward Calorimeter(FoCal) in ALICE. FoCal is a possible up-grade to the ALICE experiment, which could be installed during LS3(Long shutdown 3) for data-taking in 2026−2028 at the LHC. The first part of the thesis is about the motivation and overview of the results achieved in the later sections of the thesis, Later chapters focuses on basics about calorimeter and detector geometry of FoCal and its description mainly about FOCAL-E, and about the simulation framework through which we are doing the analysis. In the analysis part we mainly focus on the reconstruction performance for the above said neutral mesons by extracting the signal and finding reconstruction efficiency, peak position and width for the three mesons to asses the reconstruction performance in FoCal, lastly we also see the $\frac{\eta}{\pi^0}$ ratio for the FoCal coverage in pp systems.

Contents

List of Figures

Chapter 1

Introduction

The Quark-Gluon Plasma (QGP)[4] is a state of matter that existed in the first few microseconds after the Big Bang[6]. It is created when heavy nuclei, such as lead or gold, collide at high energies. The ALICE[1] experiment at the Large Hadron Collider (LHC) is designed to study the QGP. One way to study the QGP is to measure the production of photons, neutral mesons in the forward region of the ALICE experiment. The forward region is defined as the region of the detector that is close to the beamline. The photons, neutral mesons that are produced in the forward region can be used to study the properties of the QGP in forward region as to previously measured in central region.

The measurement of high transverse momentum neutral pions in lead-lead collisions can be used to probe the hot and dense strongly interacting medium relative to proton-proton collisions away from midrapidity. The reconstruction of neutral pions in lead-lead collisions is challenging due to high multiplicity in lead-lead collisions. However, FOCAL is designed to be able to reconstruct π^0 at very high $p_T \approx$ 20 GeV/c. One of the key physics goals of FOCAL is the measurement of prompt photons in forward rapidity, which would require good two photon separation from π^0 decay which is possible due to highly granular layers of FOCAL detector.

The goal of this project is to explore the reconstruction of π^0, η, and ω meson in pp collisions at $\sqrt{s} = 14$ TeV in Forward Calorimeter in ALICE. The reconstruction of π^0, η, and ω would be essential for the measurements of prompt photons which are of great interest for the physics program of FOCAL[2].

1.1 Motivation

FOCAL is a proposed upgrade to the ALICE[1] experiment at LHC that is planned to be installed during LS3. FOCAL is uniquely placed to probe low-x ($x \approx 10^{-6}$) (x is the momentum fraction of the parton with respect to hadron) physics at moderate Q^2(Q^2 is the momentum transfer between the two colliding hadrons). Key probes to explore these physics are isolated photons, π^0, jets etc

To make a measurement on prompt photons, we need a good decay photon rejection coming from hadron decays to make precise measurements. In the FOCAL Letter of Intent[2], π^0 reconstruction have been studied in a BOX generator, which is a moving particle gun and a π^0 decay is considered to be a single event. In this thesis we focus on π^0, η, and ω reconstruction via their photon decay channel in p-p collisions for a more realistic detector response, which would allow for greater precision measurement of prompt photons in pp collisions.

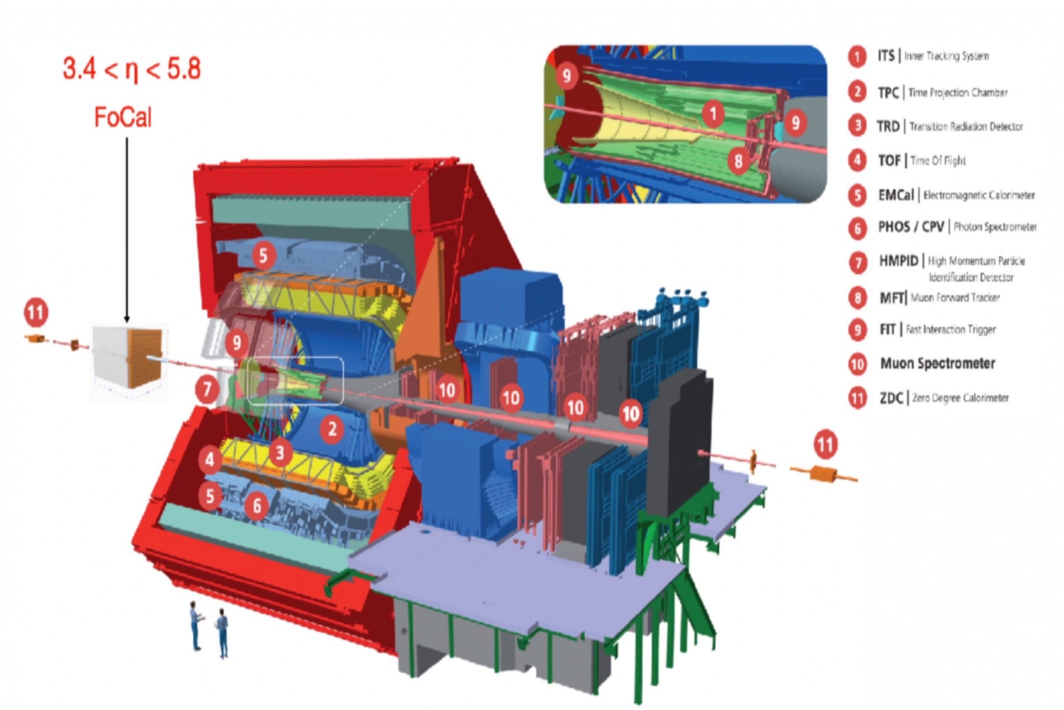

FIGURE 1.1: Schematic view of ALICE detector with its sub-detectors including FOCAL

1.1.1 Overview of Thesis

Here we will outline a brief overview of the agenda and results for rest of the thesis:

- **Chapter 2** focuses on description of FOCAL detector, its physics goals and its placement within ALICE detector in Run4. Basics about calorimeter, Simulation framework and some details about the clustering algorithm is also discussed
- **Chapter 3** focuses on analysis and results for the reconstruction of π^0, η, and ω meson in pp collision. It describes in great detail about various steps involved in reaching the final result
- **Chapter 4** is a Summary and Outlook section for the thesis
- **Chapter 5** contains supplement plots for the readers reference

In this thesis the reconstruction of π^0, η, and ω meson will be demonstrated in depth in pp collisions via the following decay channels, $\pi^0 \rightarrow \gamma + \gamma$, $\eta \rightarrow \gamma + \gamma$ and $\omega \rightarrow \pi^0 + \gamma$.

Invariant mass reconstruction method is used, background generation techniques and their comparison is also discussed, signal extraction via background subtraction and peak and width positions and Acceptance×Efficiency as a function of p_T in different psuedorapidity slices of FOCAL coverage is also shown. Lastly we try to see $\frac{Purity}{Efficiency}$ corrected yields for π^0 and η and see the $\frac{\eta}{\pi^0}$ ratio as a function of p_T in FOCAL coverage.

Chapter 2

Forward Calorimeter

2.1 Forward Calorimeter(FOCAL)

FoCal[2] is a new addition to the ALICE[1] experiment at LHC that is planned to be installed during LS3. It will be used for data collection in Run4 from 2026 to 2028 and has a pseudorapidity range of $3.4 < \eta < 5.8$. FoCal expands on ALICE's original purpose of examining hot and dense partonic matter by enabling the exploration of small-x parton structures of nucleons and nuclei. One of FoCal's significant capabilities is the ability to detect π^0 decays at forward rapidity, which can reconstruct photon pairs separated by a few mm on the detector's surface.

2.1.1 Physics Goals of FOCAL

Here in this thesis I would not be going in depth with the physics goals of FOCAL, since in this thesis we are focused on reconstruction performance of neutral mesons, a brief idea about the physics goals of FOCAL is mentioned below,

- Quantify the nuclear modification of the gluon density in nuclei at small-x and Q^2 by measuring isolated photons in pp and p-Pb collisions
- Investigate non-linear QCD evolution by measuring azimuthal $\pi^0 - \pi^0$ correlations in pp and p-Pb collisions
- Investigate the origin of long range flow-like correlations by correlating neutral meson production over large range rapidity in pp and p-Pb collisions
- Quantify parton energy loss at forward rapidity by measuring high p_T neutral pion production in Pb-Pb collisions

The main purpose of the Forward Calorimeter (FoCal) is to identify isolated photons in pp and p-Pb collisions at forward rapidity. Isolated photons are ideal for studying partons because they couple directly to quarks and are not influenced by final state effects and fragmentation, unlike hadrons. To achieve this, FoCal is made up of a finely granular Si+W calorimeter with excellent energy resolution.
Additionally, it has the capability to differentiate decay photons from neutral pions and prompt photons.

2.1.2 FOCAL conceptual design

FOCAL consists of Electromagnetic as well as Hadronic calorimeter, and there are two major challenging measurements of the anticipated physics program of FOCAL,

- The measurement of direct photons in pp and p–Pb collisions at forward rapidity to explore the small-x structure of protons and nuclei at high energy

- The measurement of high transverse momentum neutral pions in Pb–Pb collisions, and their modification relative to pp collisions, to probe the hot and dense strongly interacting medium away from midrapidity.

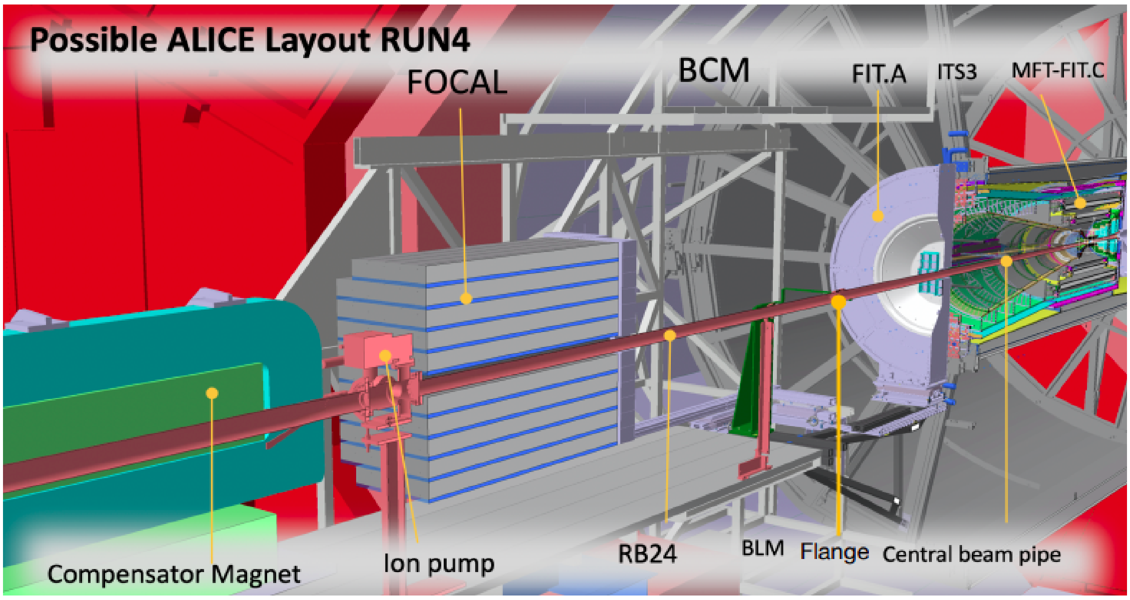

FIGURE 2.1: Possible location of FOCAL detector in ALICE in Run4

Due to large rapidity requirements of FOCAL it requires placement near to beam pipe, and since particle density is high due to kinematic boost, it is favourable to position the detector at a distance from the primary interaction vertex. FOCAL-E is placed at z = 7m from the interaction vertex and FOCAL-H is placed just behind FOCAL-E and has a psuedorapidity coverage of $3.4 < \eta < 5.8$.

For FOCAL-E, Si+W sampling calorimeter is designed and for FOCAL-H different implantations of sampling structutre is being considered such as sandwich-type(scintillator plates) and spaghetti-type(scintillator fibers) detector.

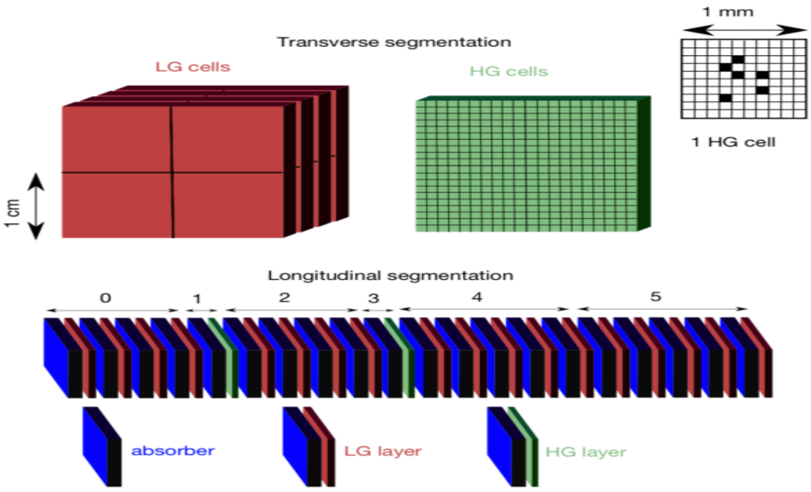

FIGURE 2.2: Schematic view of the structure of the FoCal-E detector layers

2.1.3 FOCAL-E design

For FOCAL-E a small shower size is necessary to minimize occupancy effects and to optimize the photon shower separation. Due to this Tungsten(W) was chosen as a choice of absorber material due to its small Molière[1] radius R_M and radiation length X_0, with values of $R_M = 9$ mm and $X_0 = 3.5$ mm. FOCAL will contain two different Silicon readout technologies and Tungsten as absorber material,

- Pad layers, with transverse cell sizes of $\approx 1cm^2 \approx R_M^2$
- Pixel layers, with digital readout and a cell size of $\approx 30 \times 30\ \mu m^2$, i.e. much smaller than the Molière radius, read out independently

Figure 2.3 shows the cluster XY distribution for a pp collision in the FoCal detector. The image reveals the presence of cold plates, which are dead zones used for cooling within the detector. As expected, the particle density decreases as we move away from the beam pipe, and the distribution is symmetric in the azimuthal plane.

[1]Molière radius is the radius of a cylinder containing on average 90% of the EM shower's energy deposition by e or γ.

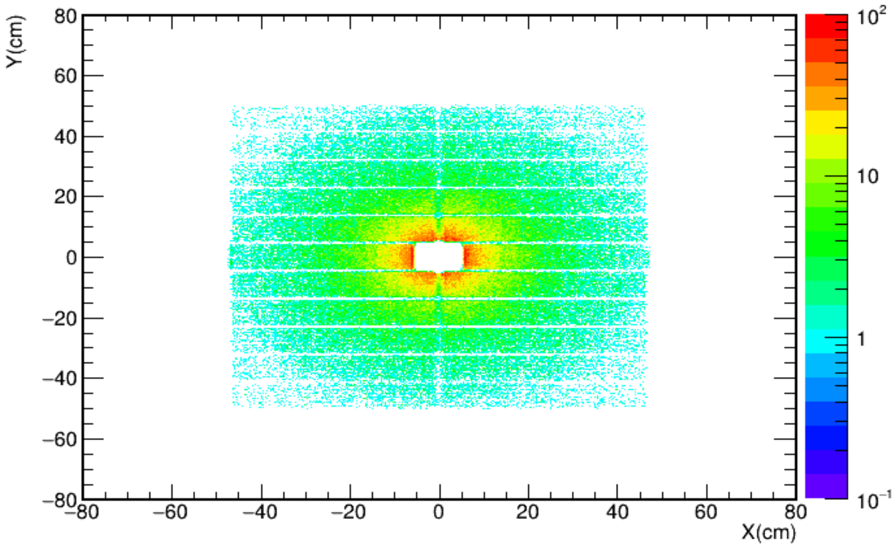

FIGURE 2.3: Cluster XY position for pp collision

However, due to the box shape of the detector, there is a loss of acceptance near the beam pipe in the very forward regions. This effect is observed in later sections of the analysis on neutral mesons efficiency. Figure 2.4 illustrates the psuedorapidity distribution of calorimeter clusters in FoCal for pp collision at 14 TeV for 50k events.

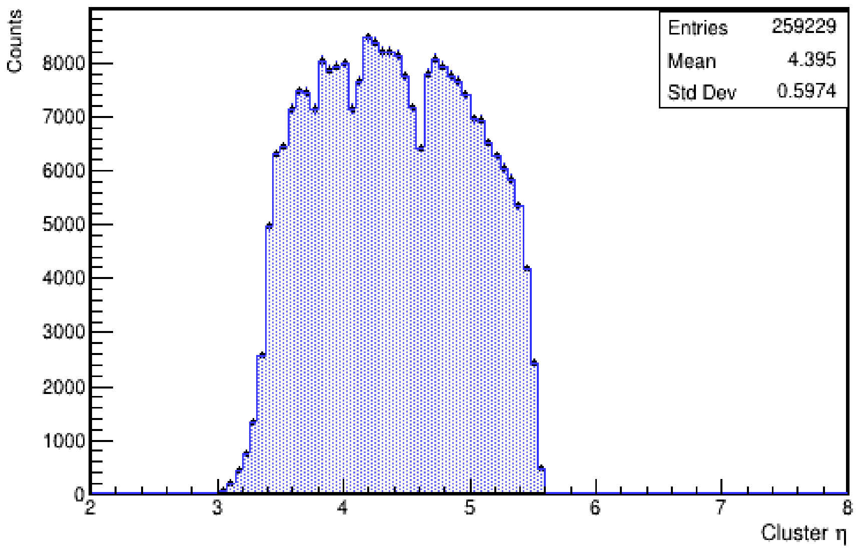

FIGURE 2.4: Psuedorapidity distribution of cluster in pp collision in FOCAL

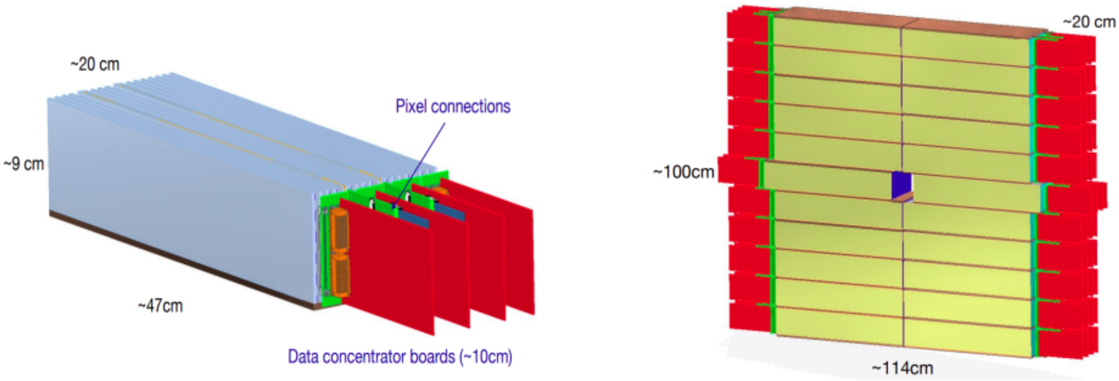

FIGURE 2.5: FoCal-E 22 modules, each 18 Pad + 2 Pixel layers

Figure 2.5 shows the FoCal-E detector design with very nice figures about layers in single modules and their dimensions.

2.2 Calorimetry details

Since we are discussing about Forward Calorimeter, it is only fair we discuss in brief about calorimetry. In particle physics, the term "calorimeter" is used to describe a device that absorbs a substantial fraction of the energy of an incident particle and produces a signal with amplitude proportional to that energy, in case of sampling calorimeter it can be split into active regions and inactive regions. The high energy particles traversing active regions cause ionization that results in charged particles that drift to anodes. The current these drifting particles produce is measured and converted into an energy measurement. Calorimeters are divided in two sections,

- Electromagnetic calorimeter: It measures the energy of light electromagnetic particles like $e^{\pm}, \gamma$ based on electromagnetic showers produced by bremsstrahlung and pair production.

- Hadronic calorimeter: It measures energy of hadronic particles like $\pi^{\pm}, K, p, n$, based on nuclear shower created by nuclear interactions.

2.2.1 Electromagnetic Showers

At higher energies (above 1 GeV), electrons, positrons, and photons interact in a similar way. Photons interact through pair production (the production of electrons and positrons), while electrons and positrons interact via bremsstrahlung (creating photons). These created particles undergo more reactions, creating a larger shower of electrons, positrons, and photons. The lateral spread of EM showers is more collimated than hadronic showers. For EM showers, this collimation is quantified by the Moliere radius, which contains 90% of the energy.

2.2.2 Hadronic Showers

The hadrons produced in a hadronic shower can interact with each other and with the matter in the shower, creating a cascade of particles. The shower continues until the hadrons have lost all of their energy.

- **Hadronic showers are much more complex than electromagnetic showers.** This is because hadrons can interact with each other and with the matter in the shower in a variety of ways.

- **Hadronic showers have a larger lateral spread than electromagnetic showers.** This is because the hadrons produced in a hadronic shower can travel in a variety of directions.

- **Hadronic showers have a longer penetration depth than electromagnetic showers.** This is because hadrons are more likely to interact with matter than photons.

2.2.3 Types of Calorimeter

Calorimeters designed for high energy physics experiments may be broadly classified into one of the two types sampling calorimeters and homogeneous calorimeters. Sampling calorimeter consists of layers of a dense passive absorber(used for shower development) such as lead or copper intertwined with active detector layers(used for signal collection) such as silicon plastic scintillator.In homogeneous calorimeter a single medium serves as both absorbing medium and the detector.

- **Homogeneous:** Single medium for shower development and signal collection. Materials used are, Organic Scintillators ,Ar,Xe
- **Sampling:** It consists of alternate absorber and detector layers, absorber layer contribute to shower development and active detector layer to signal collection. Materials used are, Pb,Cu etc for Absorber layer and Scintillator for detector layer

2.2.4 Energy resolution of Calorimeter

The energy dependence of the energy resolution may be parameterized as the quadratic sum of three terms :

$$\frac{\sigma_E}{E_0} = \frac{a}{\sqrt{E_0}} \oplus \frac{b}{E_0} \oplus c$$

The first term, with coefficient a, is the ”stochastic term”, arising from fluctuations in the number of signal generating processes(together with possible additional effects such as fluctuations in the measurement of that signal).

The second term with coefficient b, is usually referred to as the noise term.It receives contributions not only from the noise in readout electronics but also from effects as pile-up”.

The third term is constant term with coefficient c,it arises from several effects such as imperfections in calorimeter construction,fluctuations in longitudinal energy containment,channel to channel calibration errors.

2.3 Simulation framework

- Simulations are generated using event generators such as Pythia[7],HIJING[5],Particle Gun etc.
- Digitization of hits is done, after the generated particles are passed through the detector geometry produced by GEANT3[3]
- Digitized signal is then converted to clusters using clusterization algorithms.
- Package is based on AliRoot framework, to be moved to O2 framework in upcoming updates
- Clustering alogorithm is implemented for FOCAL-E, ongoing work is done for FOCAL-H clusterizer

2.3.1 Clustering Algorithm

Cluster algorithm is a method for finding clusters of energy deposits in a calorimeter. The cluster algorithm is designed to find clusters of energy deposits that are caused by particles. The algorithm works by taking into account the shower shape of particles. The shower shape is the way that the energy from a particle is deposited in the calorimeter. The shower shape is different for different types of particles. Following are the steps used in clustering,

- **Find seeds:** The algorithm starts by finding seeds, which are digits[2] that are above a certain energy threshold. The energy threshold is called the SeedThreshold
- **Collect digits:** For each seed, the algorithm collects all of the digits that are within a certain radius of the seed. The radius is called the MaxRing.
- **Create clusters:** The digits that are collected together form a cluster
- **Merge and split clusters:** The algorithm then merges and splits clusters based on weights assigned by seeds to all nearby digits. The weights are calculated using a parameterized shower shape for each segment, based on a double exponential function which has been fit to single-photon simulations. The weights depend on the energy of the seed and the distance between the digit and the seed.

After the clusters have been found in each of the segments, they are combined into full detector clusters.

[2] digits are energy deposits in calorimeter cells

Chapter 3

Analysis and Results

The analyses in this thesis to reconstruct neutral mesons was done in multiple steps, I will describe in brief about each step below,

- First we discuss about reconstruction method, like decay channel used to reconstruct neutral meson,invariant mass formula etc
- Monte Carlo data sets used for event generation
- Background generation method
- Signal extraction and fitting for peak width and position values
- Matching criteria for Acceptance and Efficiency

All of the above steps are explained in great depth in upcoming sections and subsections of the chapter.

3.1 π^0 reconstruction in pp

In this thesis, π^0 reconstruction is done using invariant mass method. The decay channel used for reconstruction of π^0 is,

$$\boldsymbol{\pi^0 \rightarrow \gamma + \gamma}$$

The invariant mass is calculated using the formula

$$\boldsymbol{M_{\pi^0}^2 = 2(E_1 E_2 - \vec{p_1}.\vec{p_2})} \tag{3.1}$$

where E_1, E_2, $\vec{p_1}$ and $\vec{p_2}$ are energy and three momentum of the two decay photons. The above equation comes from solving the momentum four vector conservation equation for the π^0 decay.

3.1.1 Monte Carlo data sets used

The MC data sets used are triggered simulations. The four Pythia triggered simulations with 50k events each are pp triggered on π^0 with minumum p_T of 1,5,10,15 GeV/c. By triggering we mean that we take those events only where we get π^0 in FoCal acceptance and with p_T greater than the threshold trigger. Here all histograms are scaled to Integrated Luminosity of 10pb^{-1} using pythia cross section and number of trials, and cluster pair p_T 1-4 GeV/c is analysed in sample of threshold trigger 1 GeV/c, and 4-10 GeV/c pair p_T in 5 GeV/c, and 10-16 GeV/c pair p_T in 10 GeV/c, and 16-20 GeV/c pair p_T in 15 GeV/c.

3.1.2 Reconstruction method

The hits produced by the event generator in the ECal and HCal of the FoCal are clusterized by a clusterizer in FoCal geometry from GEANT3. In this analysis we apply a cluster energy cut of 5 GeV to remove low energy clusters for π^0 reconstruction.

We make cluster pairs in each event with all possible combinations to get signal+background invariant mass distribution using formula 3.1.

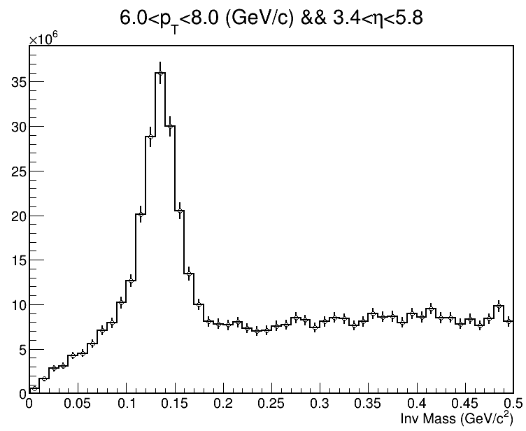

FIGURE 3.1: Invariant mass distribution for π^0

Figure 3.1 illustrates the π^0 signal and combinatorial background.

3.1.3 InEvent Rotation method

InEvent Rotation method is designed to keep as much in-event correlations between cluster pairs as possible unlike in event mixing where correlation is completely destroyed in background generation.

This method is used to describe the combinatorial background in invariant mass distributions. In this method we rotate two clusters around their combined 3-momenta by 90 degree each.

The newly rotated clusters are then paired with the rest of the clusters in the same event except the combination of the rotated clusters. This method is particularly useful in case of calorimeter where background is dependent upon in-event correlation. Figure 3.2 illustrates a comparison between Event Mixing and InEvent

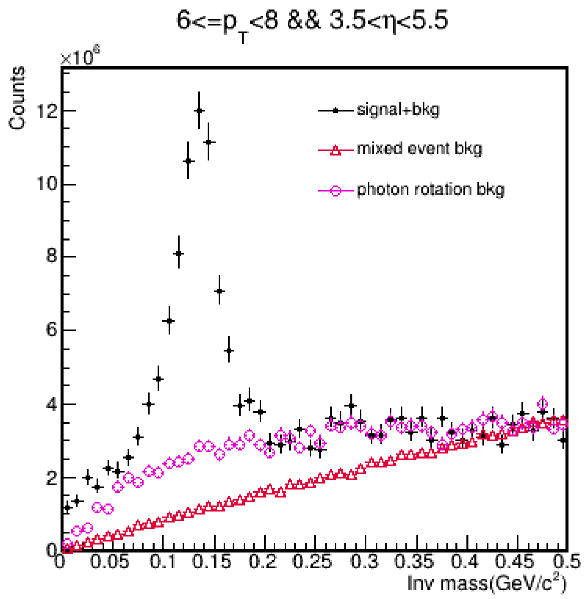

FIGURE 3.2: Background comparison between mixed event and rotation

Rotation background, as we can see that Event Mixing is unable to describe the background properly, while the rotation background seems to be in good agreement with the combinatorial background. Finally the rotation background is scaled with a factor of yield of bkg region divided by yield of generated bkg in same region.

3.1.4 Signal extraction and fitting

The signal is extracted after subtracting the rotation background from the signal+background. The extracted π^0 signal is then fitted with CrystalBall function which consists of a Gaussian core and a power law end tail.

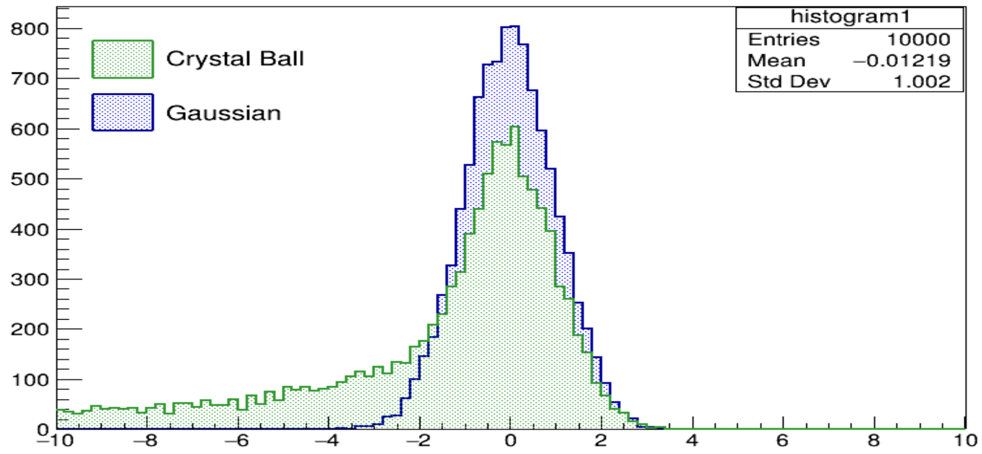

FIGURE 3.3: Comparison between Crystal Ball and Gaussian

The crystal ball function is defined as:

$$f(x;\mu,\sigma,\alpha,n,A) = \begin{cases} \frac{1}{\sqrt{2\pi}\sigma} e^{-\frac{(x-\mu)^2}{2\sigma^2}} e^{-\frac{(n/\alpha)^2}{2}} & \text{for } x-\mu > -\alpha, \\ A\left(\frac{n}{|\alpha|}\right)^n e^{-\frac{|\alpha|^2}{2n^2}} & \text{for } x-\mu \leq -\alpha, \end{cases}$$

where x is the variable, μ is the mean, σ is the standard deviation of the Gaussian core, α is the transition point, n is the power law index, and A is a normalization constant.

The choice of Crystal Ball function was made because of a tail like structure on the left side of the peak in the π^0 signal. The mean and the width of the peak are extracted from the fit parameters.

Figure 3.3 shows comparison between histograms filled with random numbers through Crystal Ball and Gaussian function for 1000 entries , the power law tail in Crystal Ball is clearly visible.

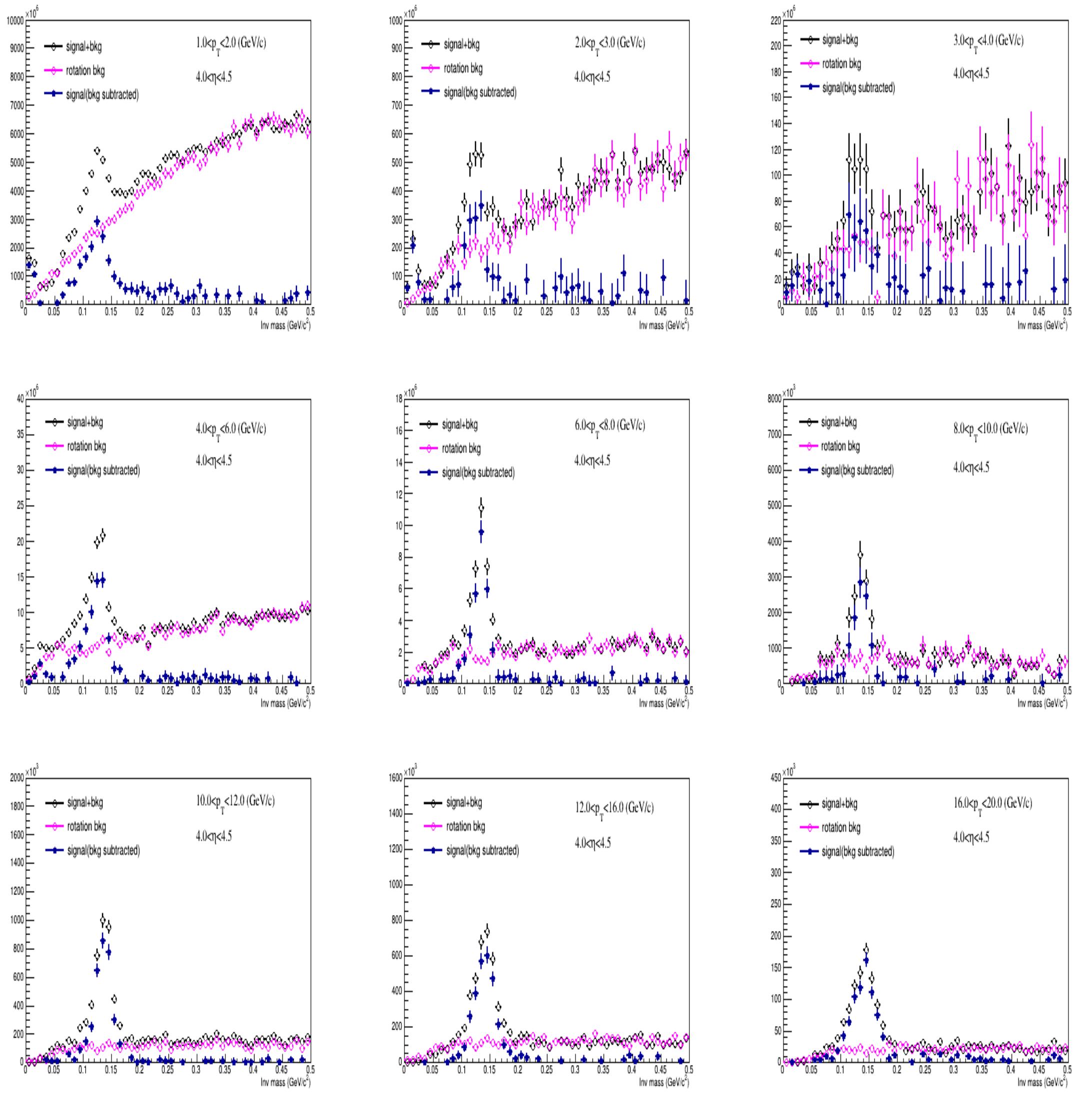

FIGURE 3.4: Invariant mass distribution for π^0 illustrating signal extraction in different p_T bins and $4.0 < \eta < 4.5$

Figure 3.4 shows the invariant mass distributions for π^0 with signal extraction for psuedorapidity range $4.0 < \eta < 4.5$. Here the black points represent signal+bkg data points, magenta points represent generated rotation bkg and the blue points represent the extracted π^0 signal. The signal extraction is also done for different psuedorapidity ranges for the FoCal, to see how the mean and the width is changing with respect to different psuedorapidity coverage, also the signal extraction is done for the whole coverage for comparison with the psuedorapidity slices.

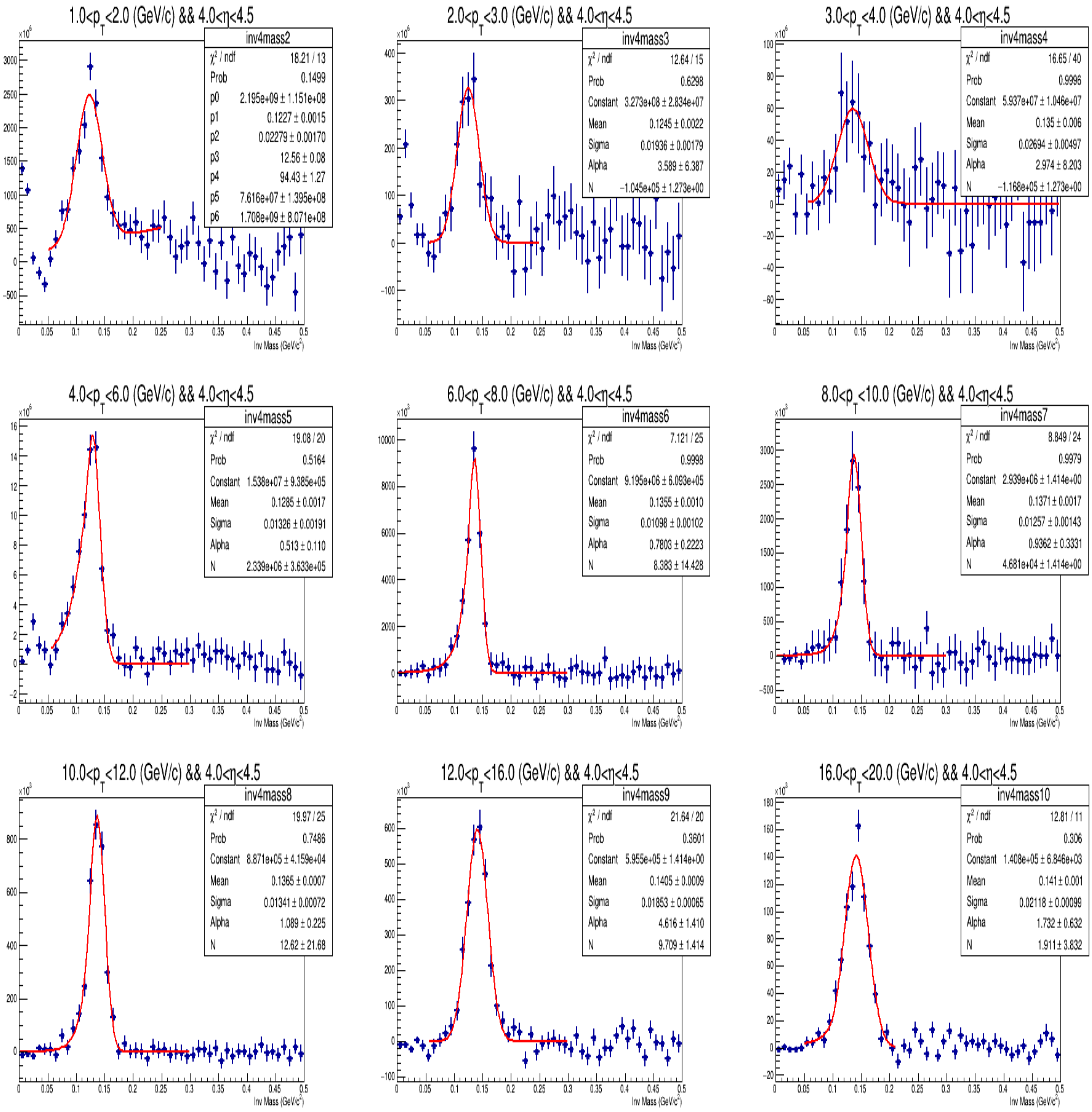

FIGURE 3.5: Fitted π^0 signal in different p_T bins and $4.0 < \eta < 4.5$

Here in figure 3.5 the fit is done for psuedorapidity range $4.0 < \eta < 4.5$, the blue points represent the extracted π^0 signal and red line represents the CrystalBall fit. The overall fit is quite good as the chi2/ndf is less than 1 in most of the p_T bins.

The fits and signal extraction plots for other psuedorapidity bins are included in the supplement section of this thesis.

3.1.5 Peak position and width for π^0 fit

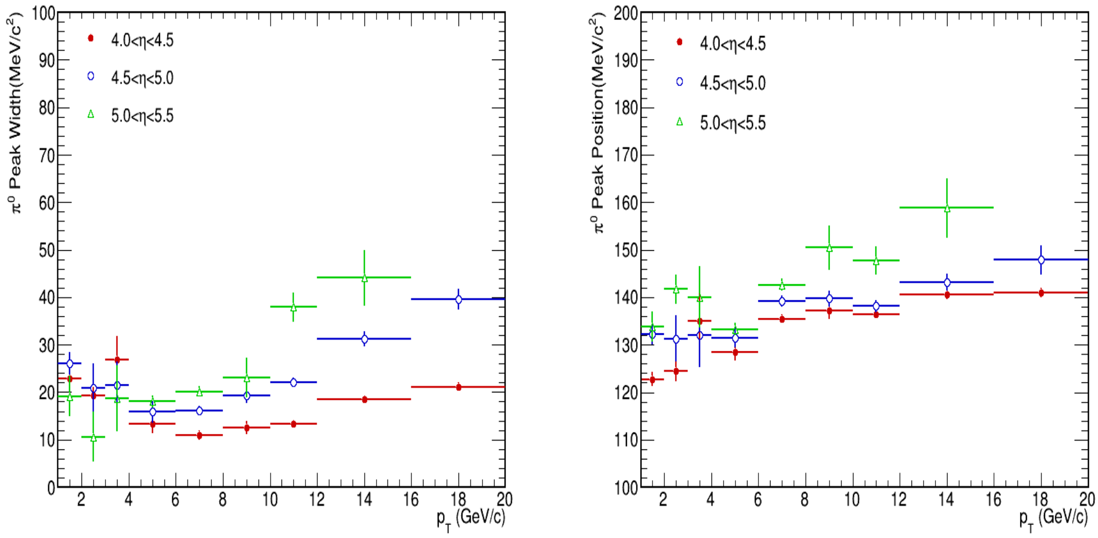

FIGURE 3.6: π^0 peak and width as a function of p_T in η bins

Figure 3.6 shows the π^0 peak width and mean position as a function of p_T and η. We were unable to reconstruct π^0 in p_T bin of 16-20 GeV for $5.0 < \eta < 5.5$ thus the missing data point in the above figure. We observe a increasing trend of peak position with increase in p_T and psuedorapidity bins, these might be due to following reasons,

- Since we are reconstructing in forward region, the opening angle will decrease as we increase more in forward psuedorapidity bins due to more boost along the beam axis, which might cause cluster merging at high p_T

- Due to smaller opening angle for π^0 the two photon clusters are less seperated, the process of seperating the two clusters in the reconstruction might induce some biases in the total reconstructed energy for the clusters and their position, this inturn will lead to a momentum dependent shift in mass which we observe

- At high p_T, π^0 are predominantly formed in jets, the two decay photon clusters due to smaller opening angle would be affected by clusters from jets around its vicinity, leading to reconstruction of π^0 at very high masses like we observe in the 3.6 figure

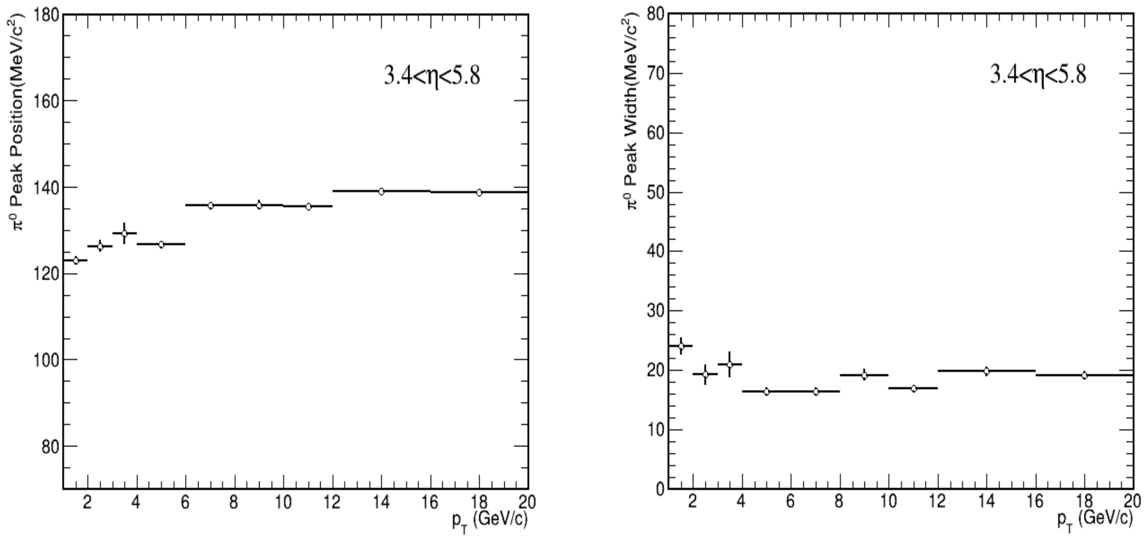

FIGURE 3.7: π^0 peak and width as a function of p_T

Figure 3.7 shows the π^0 peak width and mean position as a function of p_T for full FoCal psuedorapidity coverage. The width seems to be around 20 GeV/c^2 for the full coverage.

3.1.6 Cluster matching criteria for π^0

Clusters are matched to the closest track from the Monte Carlo stack. To match the clusters to decay photons from π^0, following matching criteria is used,

- $\Delta\phi < 0.4$ between particle to be matched and cluster, to avoid distant matching of particles with the cluster

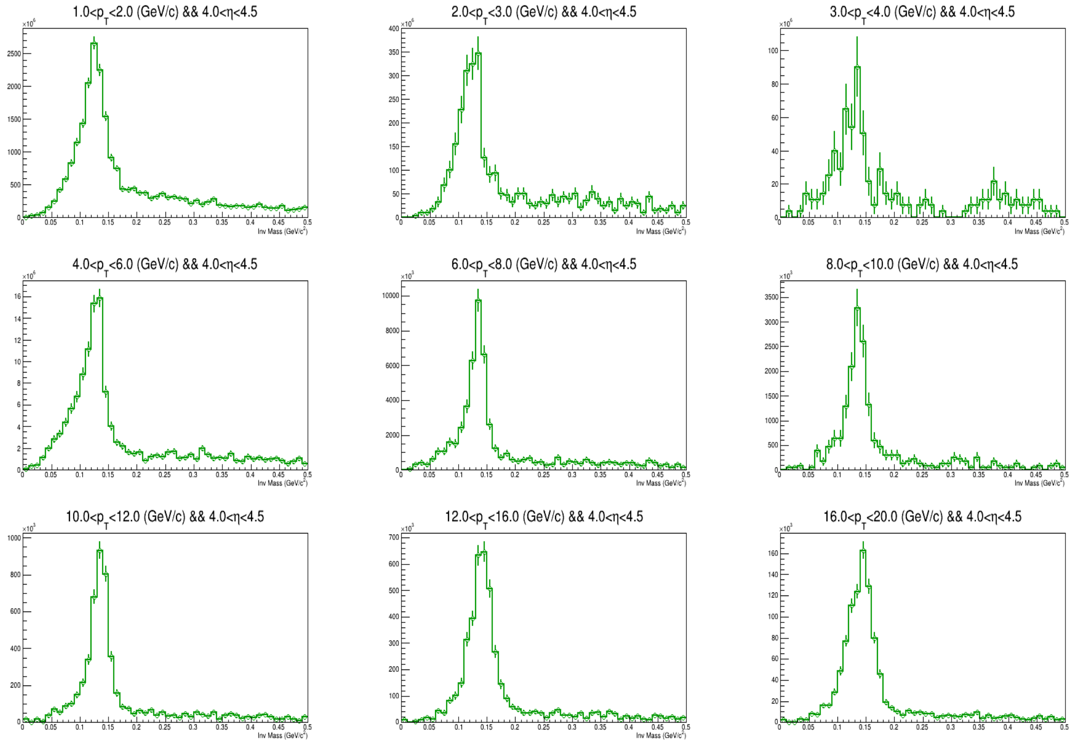

FIGURE 3.8: Matched mass distributions for π^0 in different p_T bins

- Closest track is then matched to the cluster
- After that the particle matched is checked for its PDG value, it should be photon and should come from π^0 as its mother
- Then we impose a condition that the second cluster shoud not be matched to first true photon
- Finally we check that both the clusters are matched to same π^0 as their mother

Figure 3.8 showes the matched mass distributions for π^0 for $4.0 < \eta < 4.5$, here we can see clear π^0 peak with no background, indicating a successful matching. Here by matching we essentially indicate that these cluster pairs are coming from π^0. We will use the matched cluster pairs for calculation of efficiency for π^0 in further subsection.

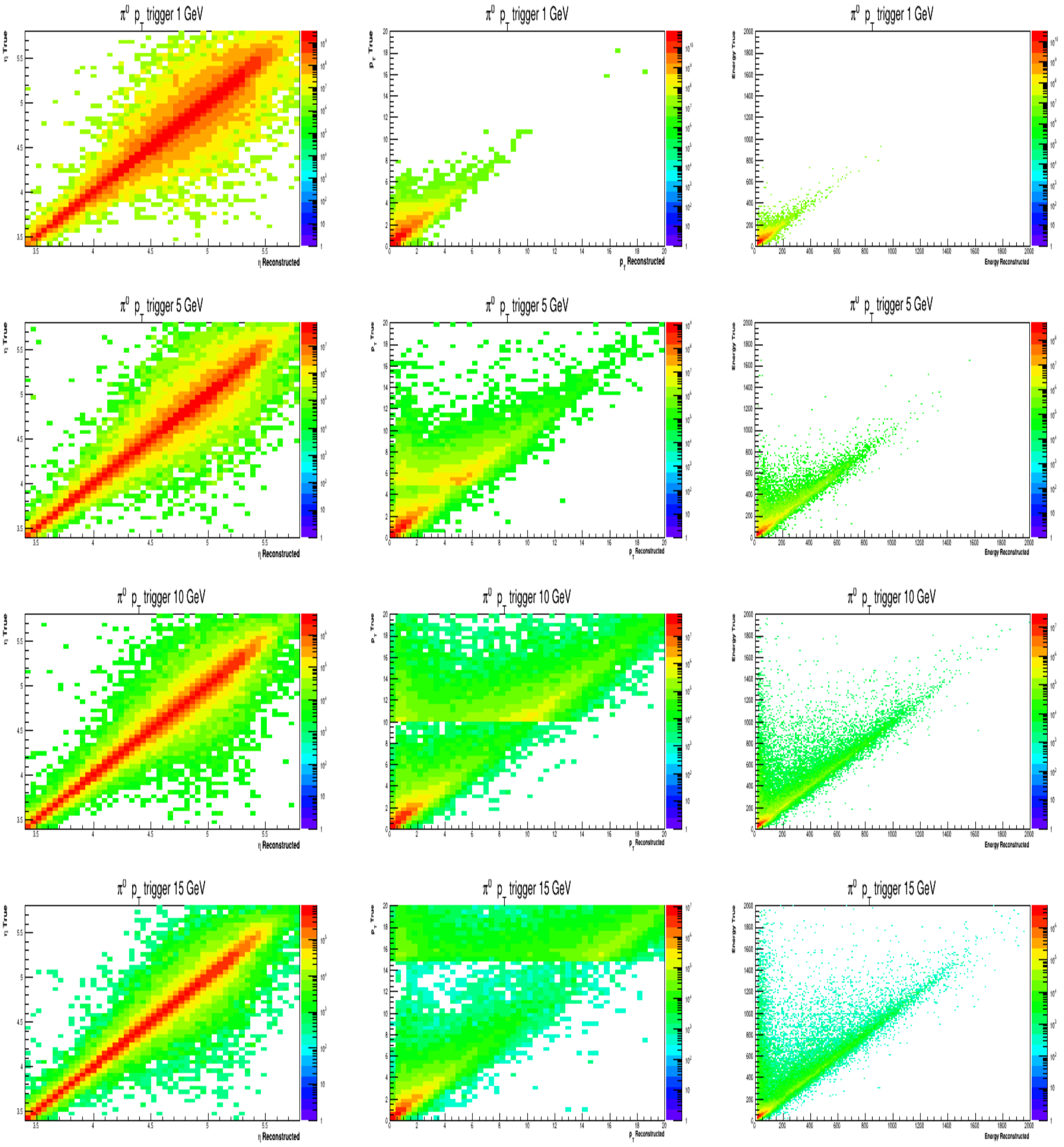

FIGURE 3.9: Reconstructed vs true π^0 for different p_T trigger samples

Figure 3.9 shows 2-d histograms for reconstructed vs true psuedorapidty,transverse momentum and energy of π^0, this would give a better idea of how effective the matching is at different p_T trigger threshold.

3.1.7 Acceptance and Efficiency for π^0

Acceptance is defined as,

$$Acceptance = \frac{\text{Number of generated } \pi^0 \text{ with decay } \gamma \text{ in FOCAL acceptance}}{\text{Number of generated } \pi^0 \text{ in FOCAL acceptance}}$$

Efficiency is defined as,

$$Efficiency = \frac{\text{Number of true } \pi^0 \text{ matched to reconstructed } \pi^0}{\text{Number of generated } \pi^0 \text{ with decay } \gamma \text{ in FOCAL acceptance}}$$

Here reconstructed π^0 is integrated from matched mass distributions over mass range $(0.05, 0.20) GeV/c^2$.

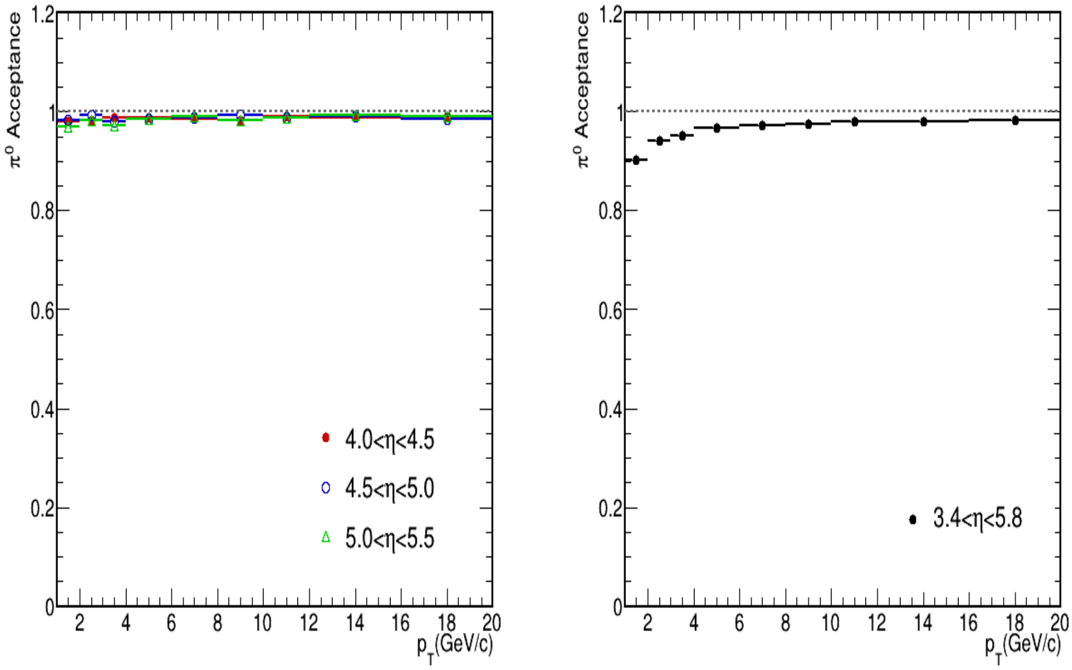

FIGURE 3.10: π^0 Kinematic Acceptance as a function of p_T in different η slices

Figure 3.10 shows π^0 Acceptance as a function of p_T for different η bins, Acceptance is over 90 percent for all p_T bins.

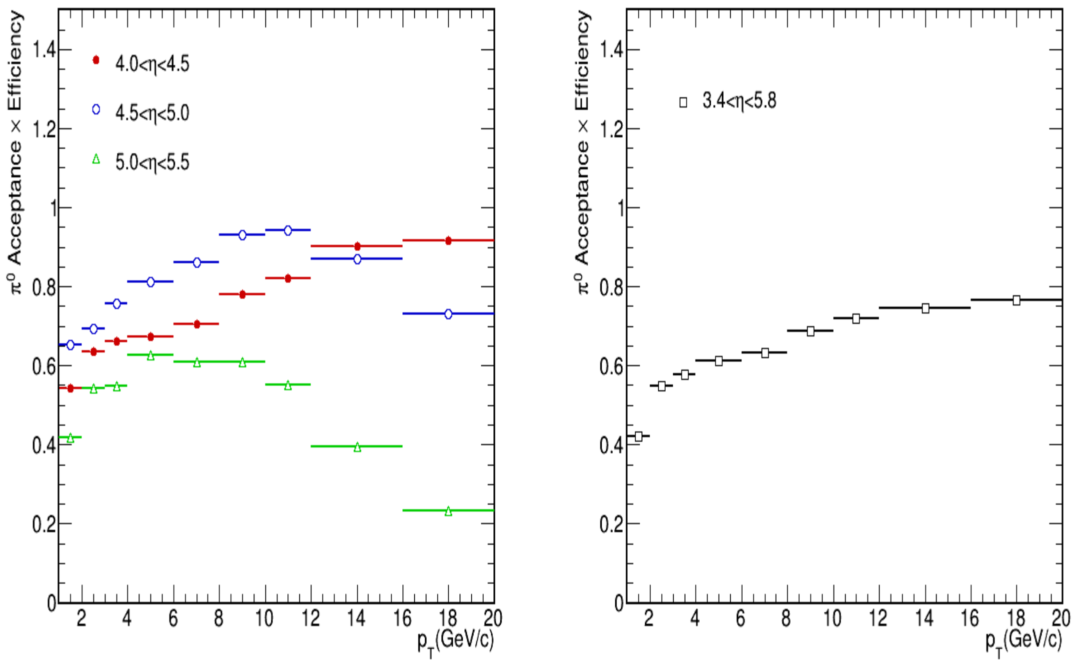

FIGURE 3.11: Acceptance*Efficiency for π^0 as a function of p_T in different η slices

Figure 3.11 shows the Acceptance*Efficiency for π^0, we see for the third η bin the efficiency is quite low due to acceptance loss and cluster merging effects.

3.2 η reconstruction in pp

In this thesis, η reconstruction is also done using invariant mass method. The decay channel used for reconstruction of η is,

$$\boldsymbol{\eta \rightarrow \gamma + \gamma}$$

The invariant mass is calculated using the formula

$$\boldsymbol{M_\eta^2 = 2(E_1E_2 - \vec{p_1}.\vec{p_2})} \tag{3.2}$$

where E_1, E_2, $\vec{p_1}$ and $\vec{p_2}$ are energy and three momentum of the two decay photons. The above equation comes from solving the momentum four vector conservation equation for the η decay.

3.2.1 Monte Carlo data sets used

Here we use the same Pythia triggered simulations for η as we had done in case of π^0 with p_T threshold of 1,5,10 and 15 GeV/c trigger. Same cluster pair p_T threshold limit is applied for η as done for π^0 simulations. Here all histograms are scaled to Integrated Luminosity of 10pb^{-1} with cross section and number of trials.

3.2.2 Reconstruction method

The hits produced by the event generator in the ECal and HCal of the FoCal are clusterized by a clusterizer in FoCal geometry from GEANT3. In this analysis we apply a cluster energy cut of 5 GeV to remove low energy clusters for η reconstruction.

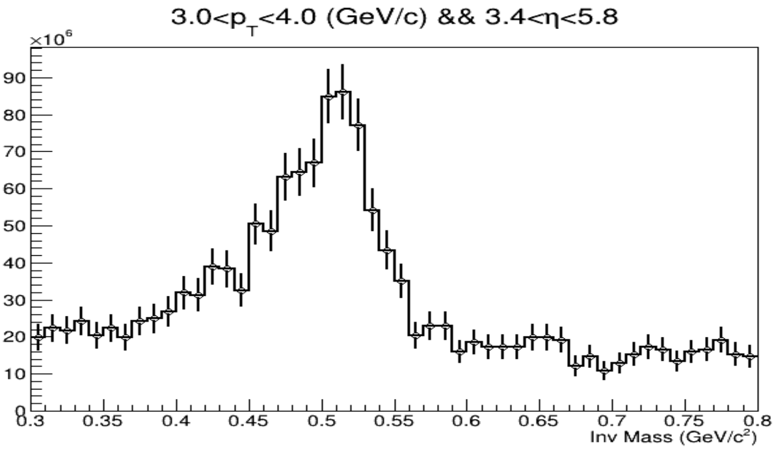

FIGURE 3.12: Invariant mass for η

We make cluster pairs in each event with all possible combinations to get signal+background invariant mass distribution using formula 3.2.

Figure 3.12 illustrates signal+bkg mass distribution for η meson.

3.2.3 Background generation and Signal extraction

We use the same InEvent rotation method to generate background as we did in the case of π^0 due to similar decay channel.Figure 3.13 shows the rotation bkg with signal extraction for η meson.

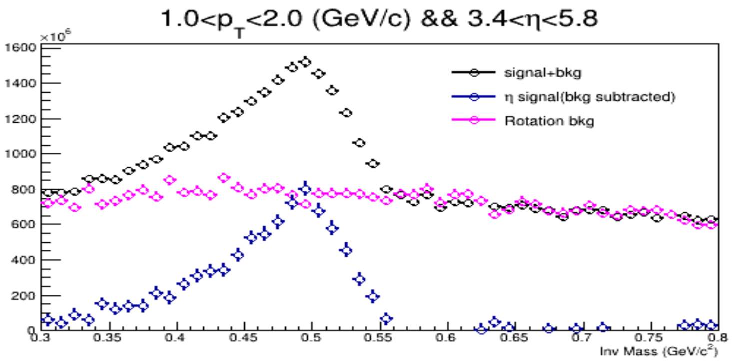

FIGURE 3.13: Rotation background for η meson

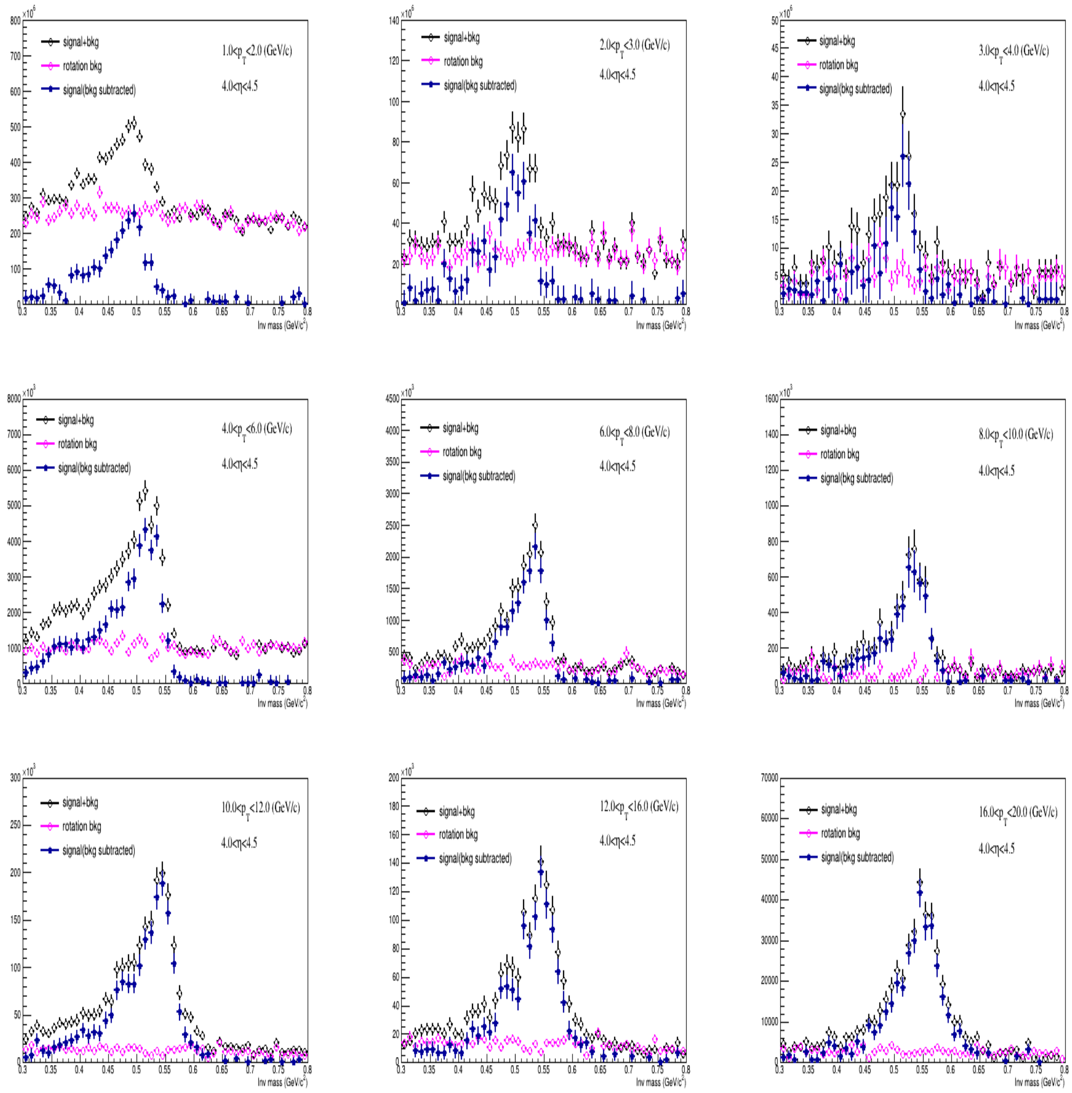

FIGURE 3.14: Invariant mass distribution for η illustrating signal extraction in different p_T bins and $4.0 < \eta < 4.5$

Figure 3.14 shows the invariant mass distribution with signal extraction for η meson in different p_T bins and psuedorapidity range of $4.0 < \eta < 4.5$. We observe that the rotation bkg is able to describe the bkg quite well in case of η meson.

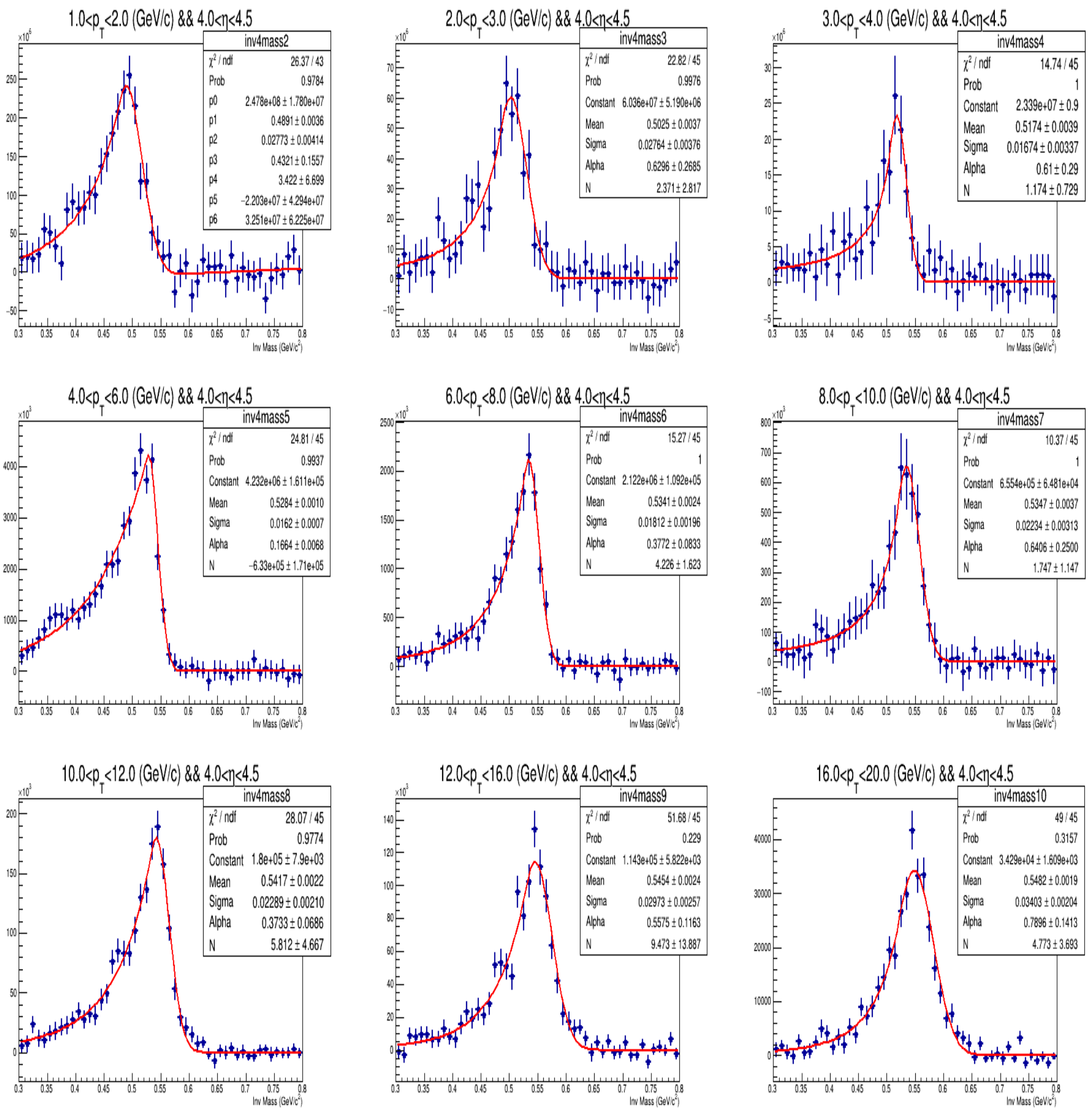

FIGURE 3.15: Fitted η signal for different p_T bins in different p_T bins and $4.0 < \eta < 4.5$

Figure 3.15 shows the fitted bkg subtracted η signal with CrystalBall fit in different p_T bins and psuedorapidity range of $4.0 < \eta < 4.5$. The overall fit is quite good for the η signal as the chi2/ndf is less than 1 in all p_T bins.

The mean and the sigma will be extracted from the fit and would be plotted as a function of p_T in later subsection. Plots for different psuedorapidity bins are provided in the supplement section.

3.2.4 Peak position and width for η fit

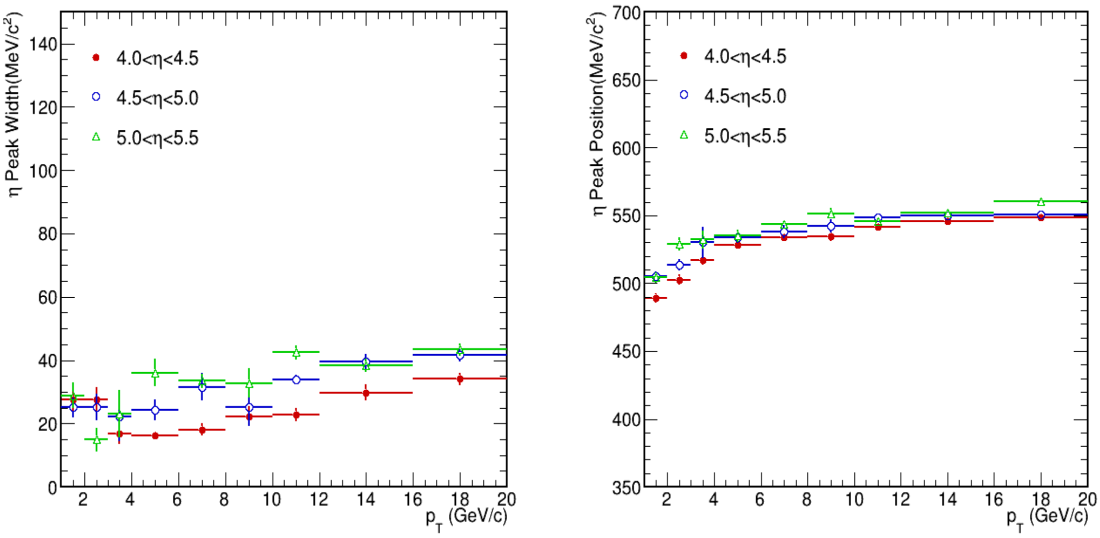

FIGURE 3.16: η peak position and width as a function p_T in different η slices

Figure 3.16 shows the η meson peak width and mean position as a function of p_T and η. Here the peak positions is not increasing is not increasing rapidly as it did in case of π^0, due to larger opening angle for decay photons of η, which help in better reconstruction of η meson.

Since high p_T η mesons are predominantly found in jets, due to larger opening angle the two decay photon clusters would be well separated from the jet cone resulting in low contributions from clusters due to jets, thus we observe a better reconstruction of η meson throught η and p_T bins.

Figure 3.17 shows the η peak and width for the full psuedorapidity coverage of the FoCal detector.

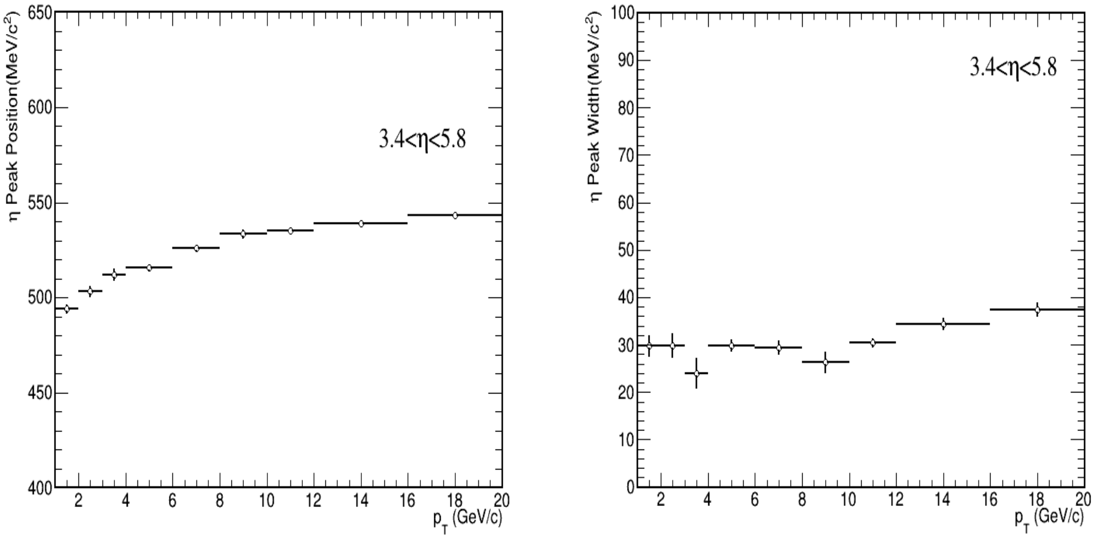

FIGURE 3.17: η peak position and width for full coverage as a function p_T in different η slices

3.2.5 Cluster matching criteria for η

Cluster matching criteria is same as that for π^0, since both have same decay channel so please refer to 3.1.6 matching criteria of π^0 for detailed text about matching. Figure 3.18 illustrates matched mass distributions for η meson for $4.0 < \eta < 4.5$. Figure 3.19 illustrates the reconstructed vs true η meson distributions for η, p_T and Energy for different p_T trigger thresholds. Reconstructed η is integrated from matched mass distributions over mass range $(0.3, 0.7)GeV/c^2$. Here we see a nice diagonal trend which indicates a successful matching between true and reconstructed η.

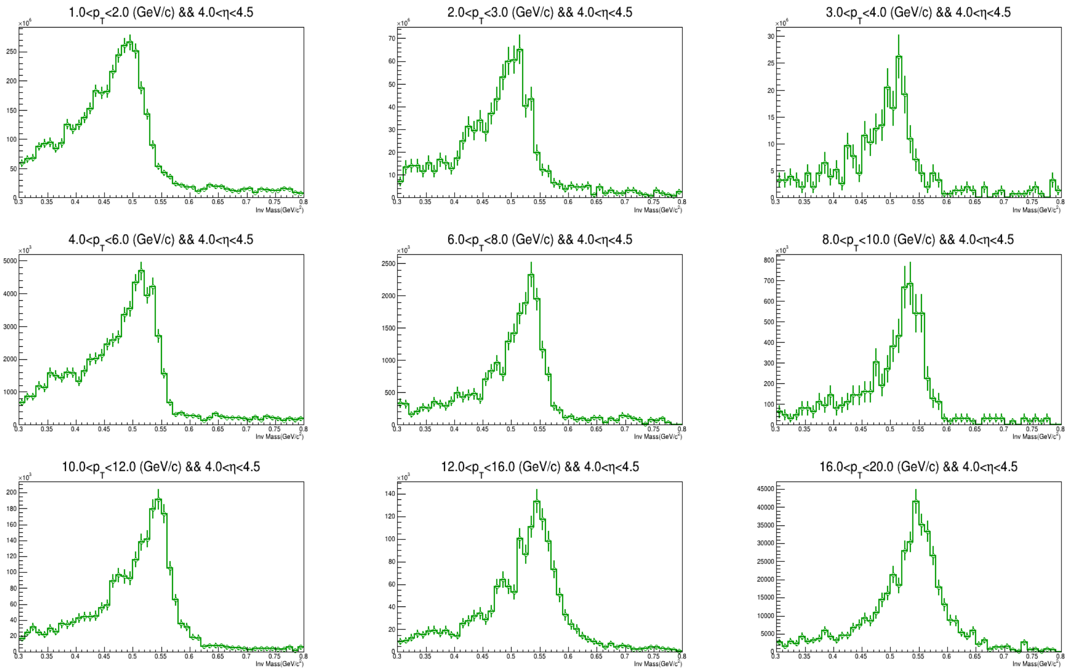

FIGURE 3.18: Matched invariant mass distributions for η meson for different p_T bins

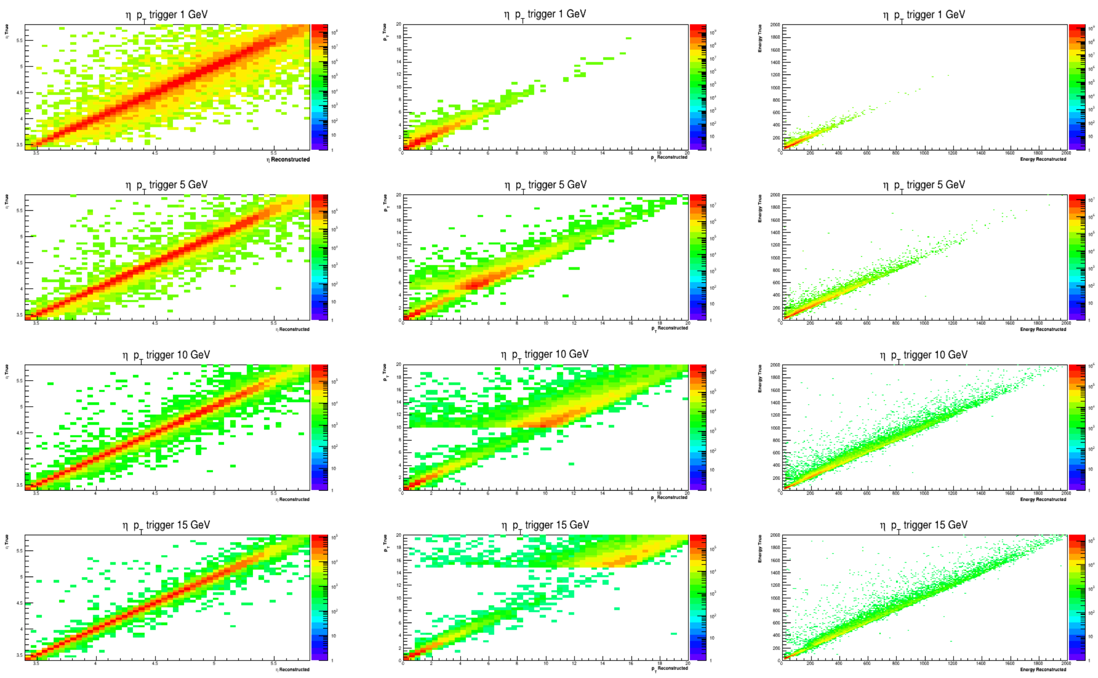

FIGURE 3.19: 2-d histograms for reconstructed vs true η for different p_T trigger samples

3.2.6 Acceptance and Efficiency for η

Acceptance is defined as,

$$Acceptance = \frac{\text{Number of generated } \eta \text{ with decay } \gamma \text{ in FOCAL acceptance}}{\text{Number of generated } \eta \text{ in FOCAL acceptance}}$$

Efficiency is defined as,

$$Efficiency = \frac{\text{Number of true } \eta \text{ matched to reconstructed } \eta}{\text{Number of generated } \eta \text{ with decay } \gamma \text{ in FOCAL acceptance}}$$

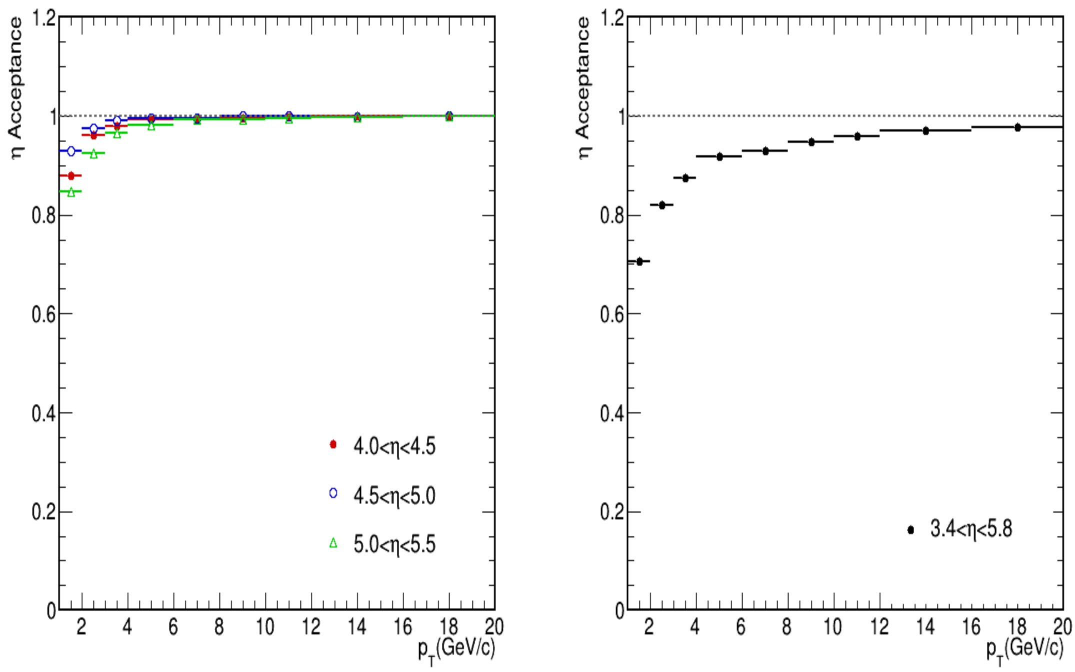

FIGURE 3.20: Kinematic Acceptance for η meson as a function of p_T in different η slices

Figure 3.20 illustrates the acceptance distribution for η meson with different p_T bins and psuedorapidity ranges. The acceptance is less as compared to π^0 possibly due to larger opening angle for decay photons of η meson compared to π^0.

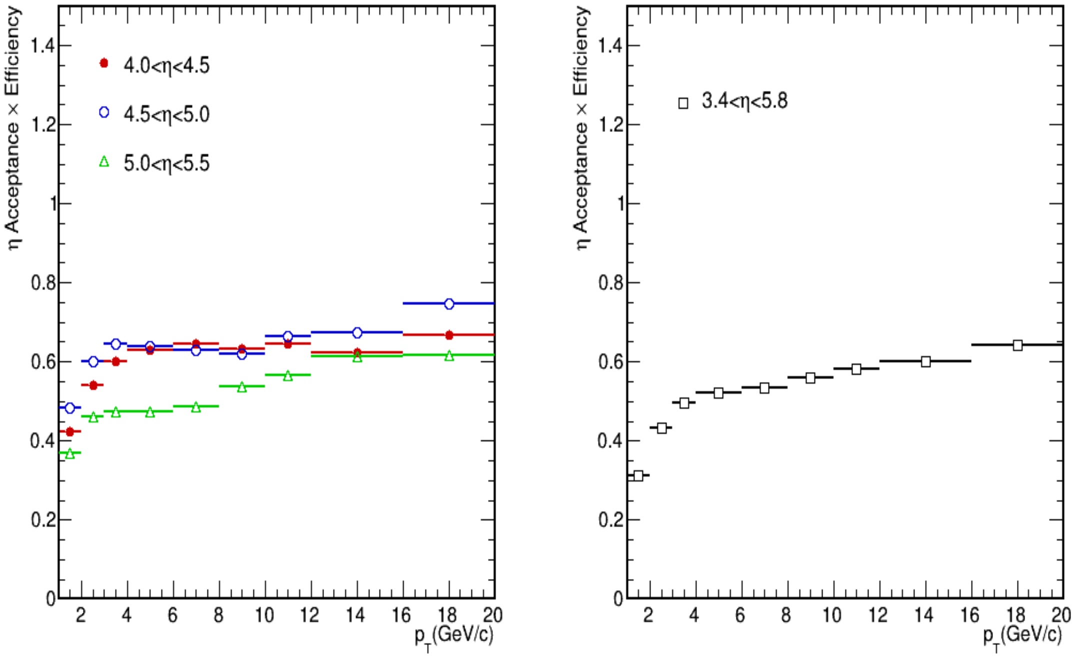

FIGURE 3.21: Acceptance*Efficiency for η meson as a function of p_T in different η slices

Figure 3.21 illustrates the Acceptance*Efficiency distribution for η meson with different p_T bins and psuedorapidity ranges. The distribution is almost flat which is due to the fact that we are able to reconstruct η meson in a better way as the peak position is not shifting with increasing p_T and psuedorapidity, the mass window we use to integrate over matched mass distribution gives a better estimate of the area under the peak compared to π^0.

3.3 ω reconstruction in pp

In this thesis, ω reconstruction is also done using invariant mass method. The decay channel used for reconstruction of ω is,

$$\boldsymbol{\omega \to \pi^0 + \gamma \to \gamma + \gamma + \gamma}$$

The invariant mass is calculated using the formula

$$\boldsymbol{M_\omega^2 = M_{\pi^0}^2 + 2(E_1 E_2 - \vec{p_1}.\vec{p_2})} \tag{3.3}$$

where E_1, E_2, $\vec{p_1}$ and $\vec{p_2}$ are energy and three momentum of the decay π^0 and γ. The above equation comes from solving the momentum four vector conservation equation for the ω decay.

3.3.1 Monte Carlo data sets used

Here we use the same Pythia triggered simulations for ω as we had done in case of π^0 with p_T threshold of 1,5,10 and 15 GeV/c trigger. Same cluster pair p_T threshold limit is applied for ω as done for π^0 simulations. Here all histograms are scaled to Integrated Luminosity of 10pb^{-1} with cross section and number of trials.

3.3.2 Reconstruction method

The hits produced by the event generator in the ECal and HCal of the FoCal are clusterized by a clusterizer in FoCal geometry from GEANT3. In this analysis we apply a cluster energy cut of 5 GeV to remove low energy clusters for ω reconstruction.

We pair 3 cluster in each event with all possible combinations to get signal+background for the three gamma invariant mass distribution using formula 3.3.

3.3.3 Background generation and Signal extraction

We use the same InEvent rotation method to generate background as we did in the case of π^0 and η with an additional change of pairing three clusters instead of two. Figure 3.22 shows the invariant mass distribution for omega meson with signal extraction for full psuedorapidity coverage.

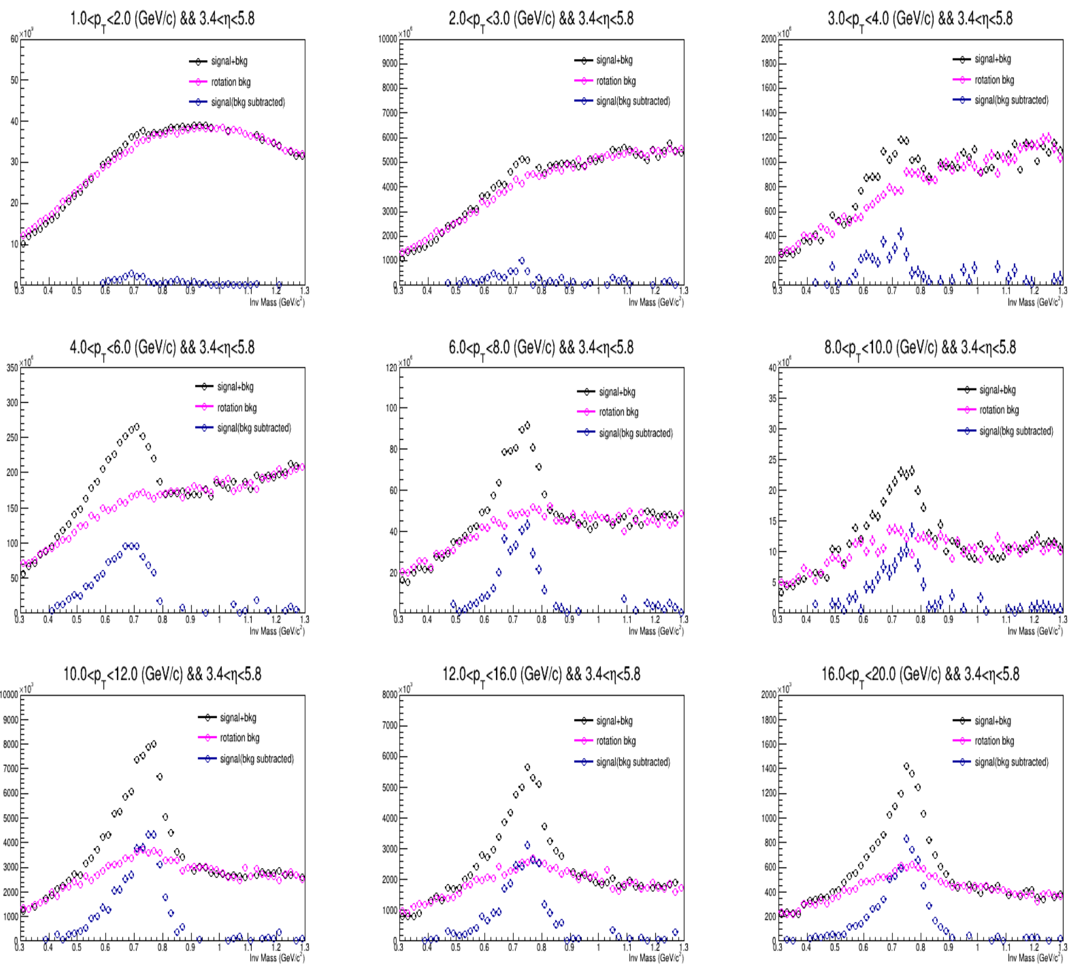

FIGURE 3.22: Invariant mass distribution for omega meson in different p_T bins and $3.4 < \eta < 5.8$

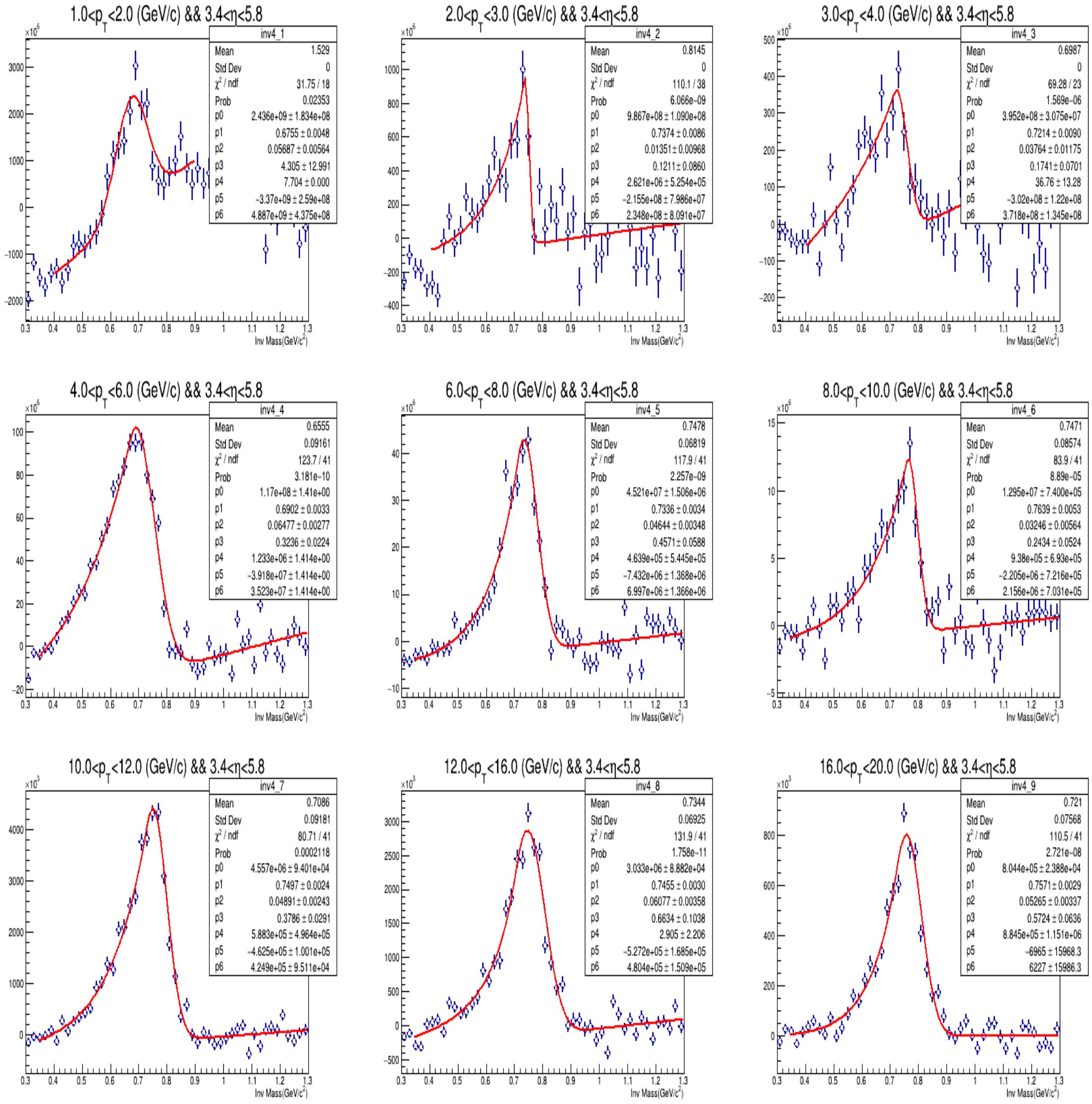

FIGURE 3.23: Fitted omega signal in different p_T bins and $3.4 < \eta < 5.8$

Here figure 3.23 illustrates fitted omega meson signal for the full psuedorapidity coverage of FoCal using a CrystalBall plus zeroth order polynomial fit which is added as a proxy for remaining correlated background under the peak.

3.3.4 Peak position and width for ω fit

Figure 3.24 illustrates the ω peak position and width as a function of p_T within full psuedorapidity coverage of FoCal.

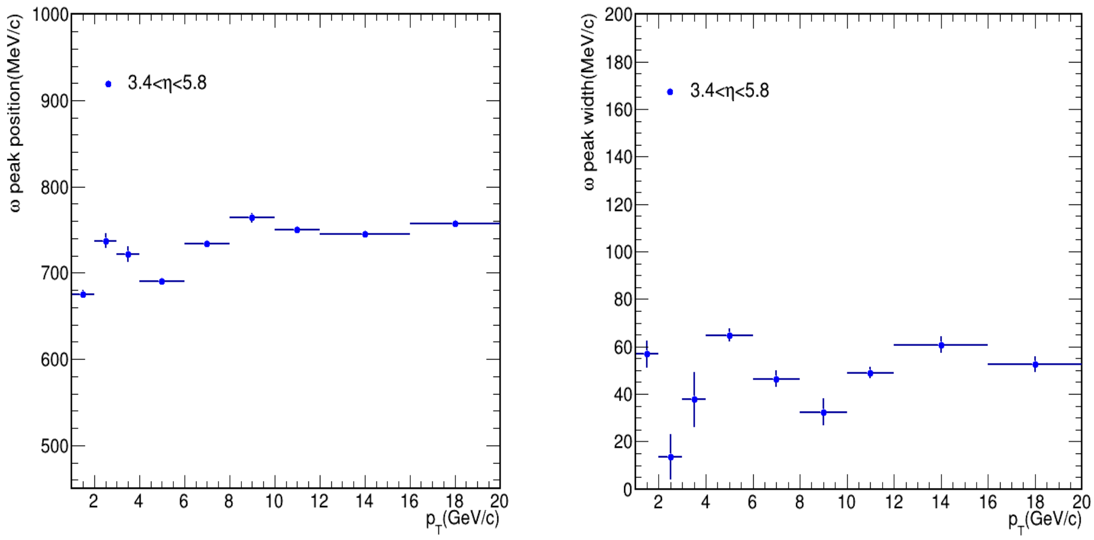

FIGURE 3.24: ω peak position and width as a function of p_T in full FOCAL η coverage

3.3.5 Cluster matching criteria for ω

Clusters are matched to the closest track from the Monte Carlo stack. To match the clusters to decay photons from ω, following matching criteria is used,

- $\Delta\phi < 0.4$ between particle to be matched and cluster, to avoid distant matching of particles with the cluster
- Closest track is then matched to the cluster
- After that the particle matched is checked for its PDG value, it should be photon and should come from π^0 as its mother and the π^0 should come from

ω as its mother if the cluster is being matched to the decay photon from π^0 which came from decay of ω

- If the cluster is checked for the photon which came from ω decay then the particle is checked for its PDG value of photon and it should come from ω as its mother
- Also no three MC photons should be same which are matched to the three clusters
- Lastly it is checked that all the three clusters are matched to same omega meson as its mother

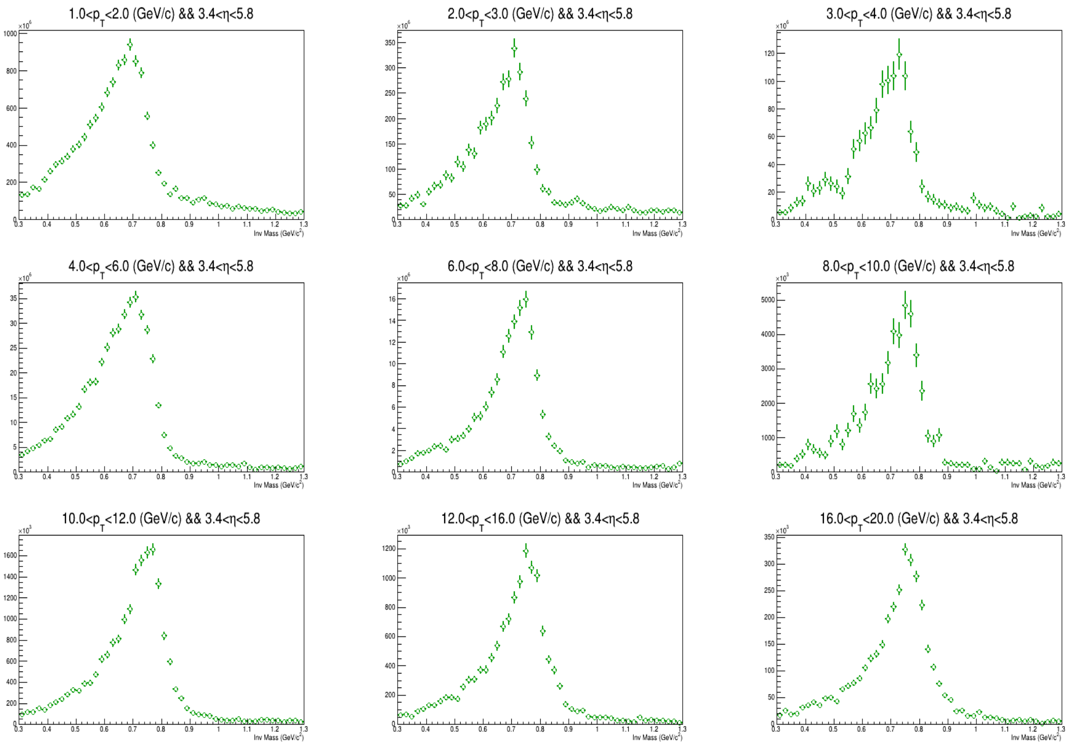

FIGURE 3.25: Matched invariant mass distributions for ω in different p_T bins and $3.4 < \eta < 5.8$

Figure 3.25 shows the matched invariant mass distributions for ω over full psuedo-rapidity coverage

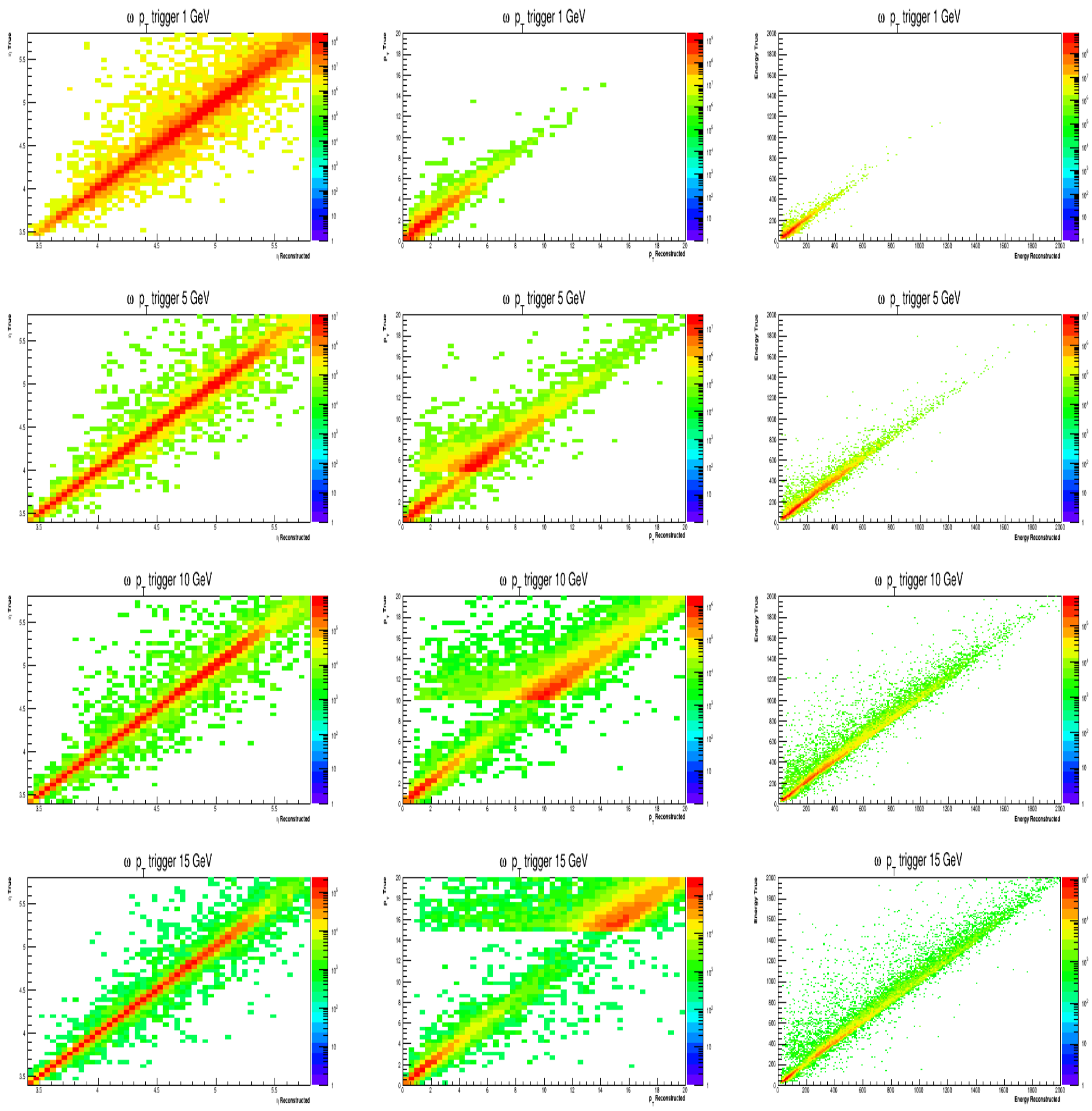

FIGURE 3.26: 2-d histograms for reconstructed vs true ω for different p_T trigger sample for $3.4 < \eta < 5.8$

Figure 3.26 illustrates the reconstructed vs true ω meson distributions for η, p_T and Energy for different p_T trigger thresholds.

Reconstructed ω is integrated from matched mass distributions over mass range $(0.4, 1.0)GeV/c^2$. Here we see a nice diagonal trend which indicates a successful matching between true and reconstructed ω.

3.3.6 Acceptance and Efficiency for ω

Acceptance is defined as,

$$Acceptance = \frac{\text{Number of generated } \omega \text{ with decay } \pi^0 \text{ and } \gamma \text{ in FOCAL acceptance}}{\text{Number of generated } \omega \text{ in FOCAL acceptance}}$$

Efficiency is defined as,

$$Efficiency = \frac{\text{Number of true } \omega \text{ matched to reconstructed } \omega}{\text{Number of generated } \omega \text{ with decay } \pi^0 \text{ and } \gamma \text{ in FOCAL acceptance}}$$

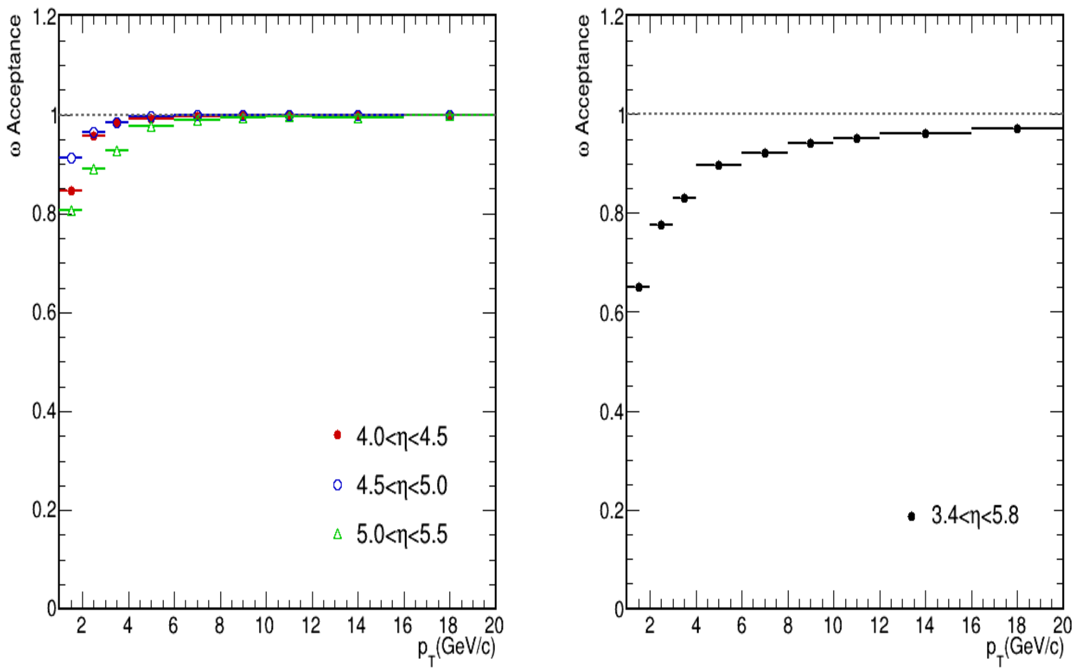

FIGURE 3.27: Kinematic Acceptance for ω meson as a function of p_T in different η slices

Figure 3.27 illustrates the acceptance distribution for ω meson with different p_T bins and psuedorapidity ranges. The acceptance is less as ω is heavier than η and π^0 meson which in-turn gives larger opening angle, thus the loss in acceptance at low p_T.

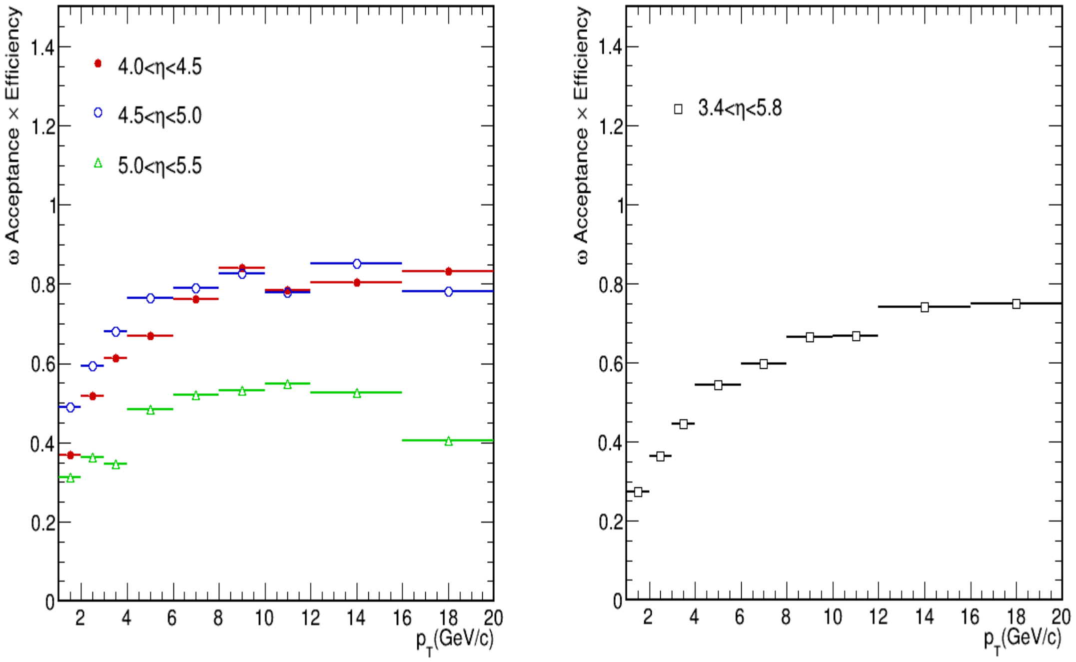

FIGURE 3.28: Acceptance*Efficiency for ω meson as a function of p_T in different η slices

Figure 3.21 illustrates the Acceptance*Efficiency distribution for ω meson with different p_T bins and psuedorapidity ranges.

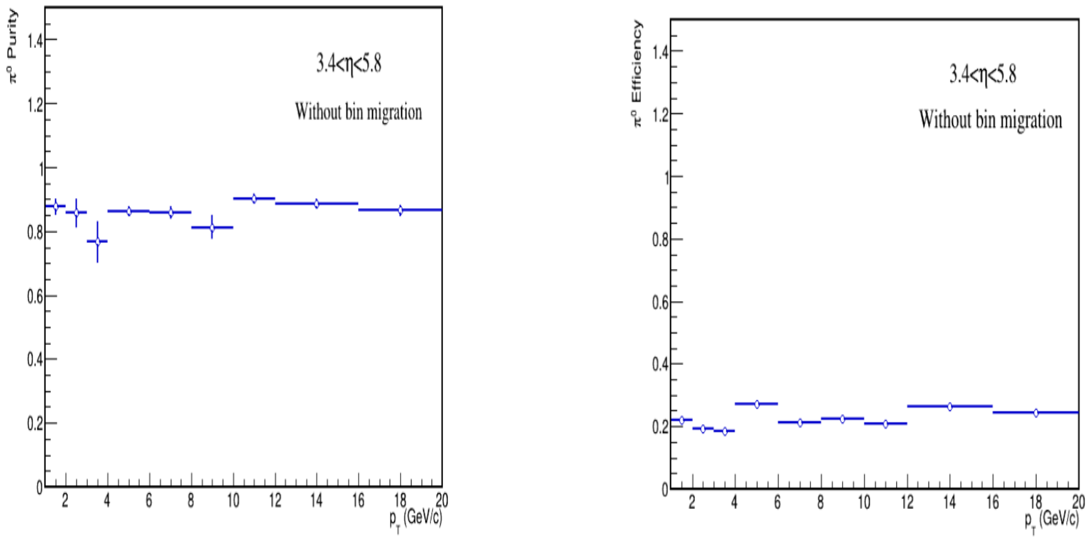

FIGURE 3.29: Efficiency and Purity for π^0 as a function of p_T

3.4 Efficiency and Purity corrected yields for π^0 and η meson

$$Efficiency = \frac{\text{Number of reconstructed } \pi^0 \text{ matched to true } \pi^0 \text{ in same } p_T \text{ bin}}{\text{Number of generated } \pi^0 \text{ with decay } \gamma \text{ and } \gamma \text{ in acceptance}}$$

$$Purity = \frac{\text{Number of reconstructed } \pi^0 \text{ matched to true } \pi^0 \text{ in same } p_T \text{ bin}}{\text{Number of } \pi^0 \text{ in } \pi^0 \text{ signal}}$$

Figure 3.29 shows the Efficiency and Purity from the above definition for π^0. Purity is very high throughout p_T, which is essential for bin by bin correction.
We multiply the matched reconstructed π^0 distribution by a factor of $\frac{Purity}{Efficiency}$, to get the corrected p_T distribution.

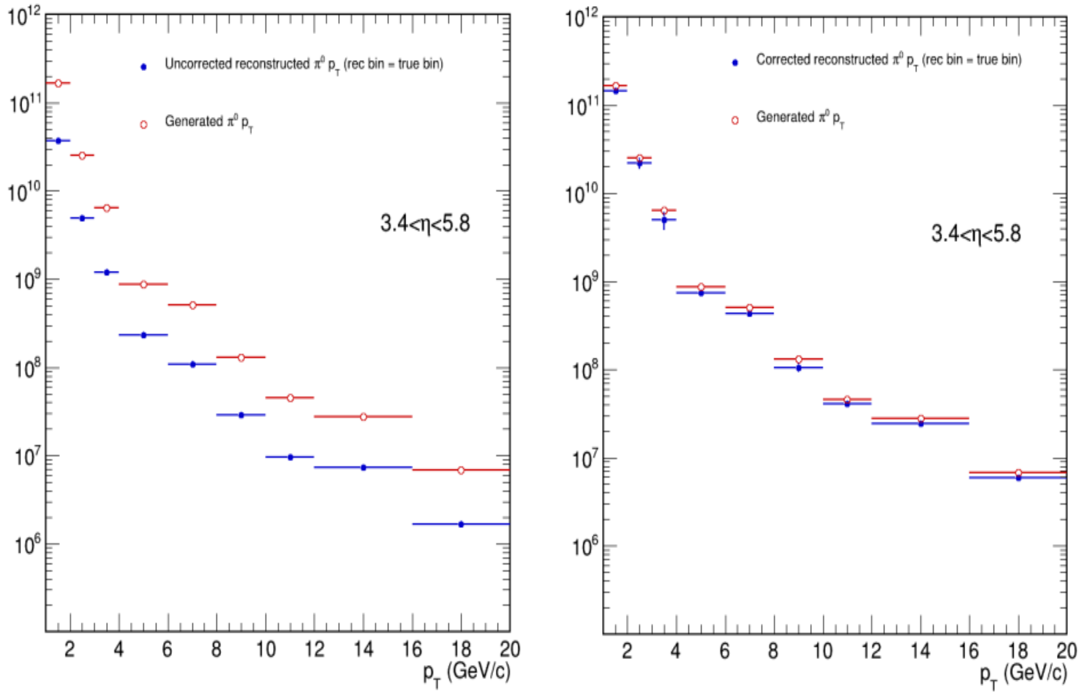

FIGURE 3.30: Purity and Efficiency corrected yields as a function of p_T for π^0

Figure 3.30 shows the Efficiency and Purity uncorrected and corrected yields for π^0.

$$Efficiency = \frac{\text{Number of reconstructed } \eta \text{ matched to true } \eta \text{ in same } p_T \text{ bin}}{\text{Number of generated } \eta \text{ with decay } \gamma \text{ and } \gamma \text{ in acceptance}}$$

$$Purity = \frac{\text{Number of reconstructed } \eta \text{ matched to true } \eta \text{ in same } p_T \text{ bin}}{\text{Number of } \eta \text{ in } \eta \text{ signal}}$$

Figure 3.31 shows the Efficiency and Purity from the above definition for η. Purity is very high throughout p_T, which is essential for bin by bin correction.

We multiply the matched reconstructed η distribution by a factor of $\frac{Purity}{Efficiency}$, to get the corrected p_T distribution.

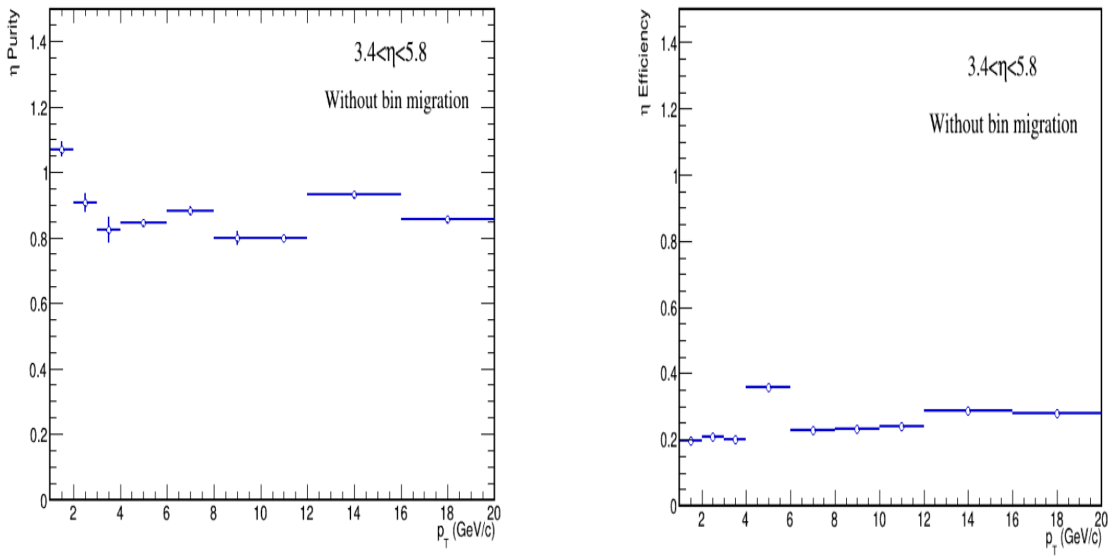

FIGURE 3.31: Efficiency and Purity for η as a function of p_T

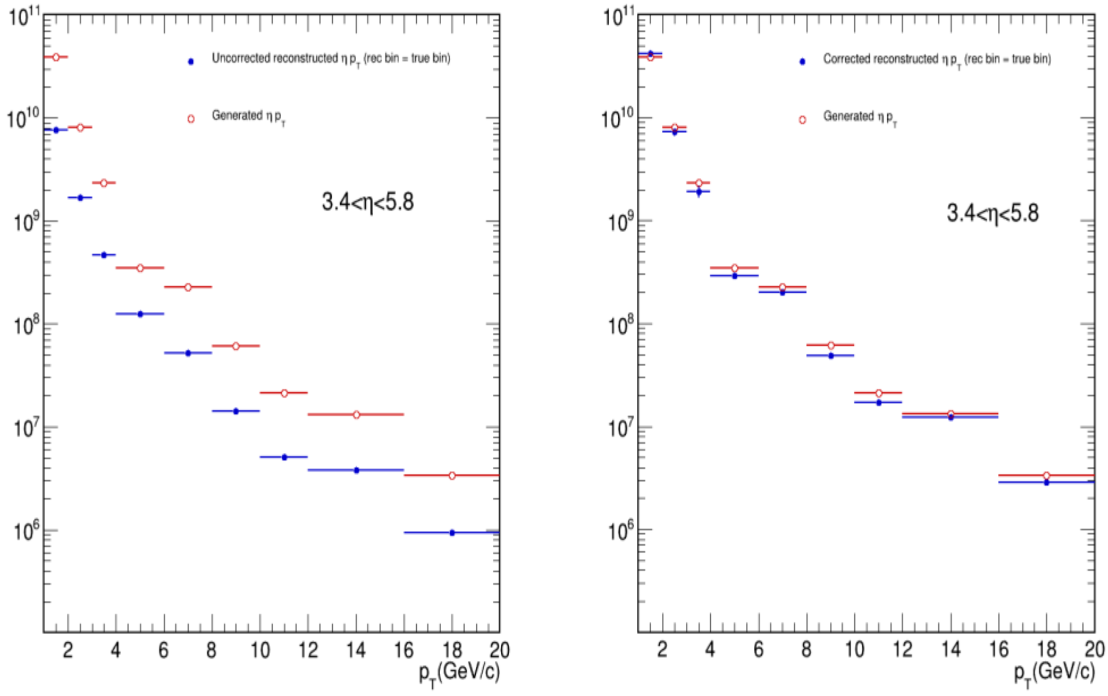

FIGURE 3.32: Purity and Efficiency corrected yields as a function of p_T for η

Figure 3.32 shows the Efficiency and Purity uncorrected and corrected yields for η.

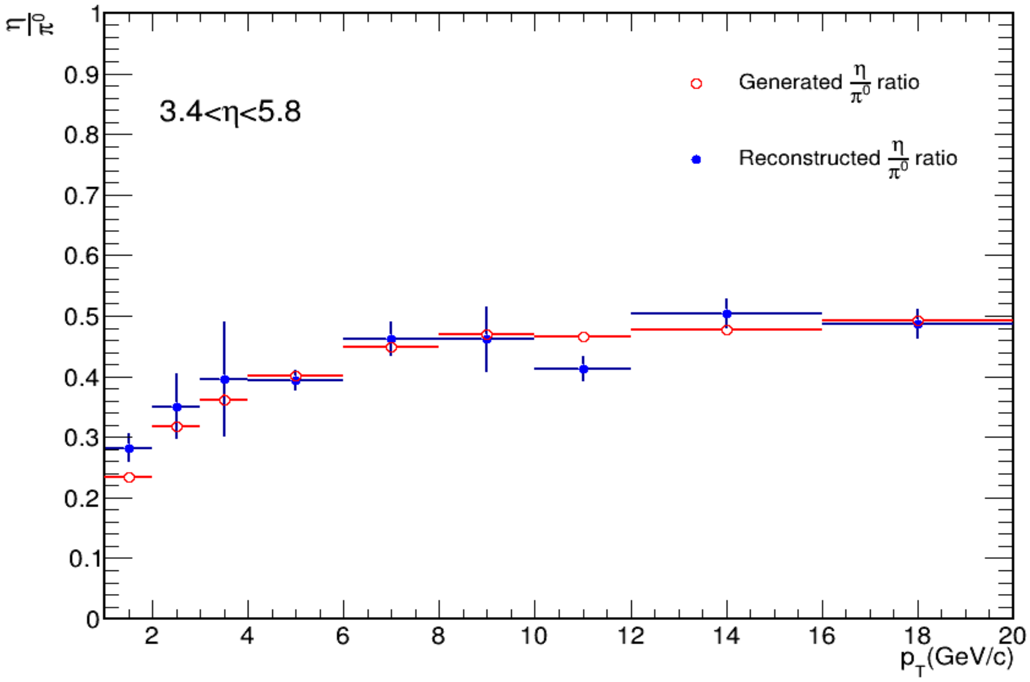

FIGURE 3.33: $\frac{\eta}{\pi^0}$ corrected yield ratio as a function of p_T

Figure 3.33 shows the $\frac{\eta}{\pi^0}$ for the generated and corrected reconstructed yield ratio with statistical errors for pp systems for the full FOCAL psuedorapidity coverage. Although these ratio don't have that much significance in simulation rather than in real data, but these provide us an insight on how the ratio and statistical errors will look in real data. This ratio can also provide insight into how the yields of η and π^0 change for pp and PbPb systems.

Chapter 4

Summary and Outlook

4.0.1 Summary

In this thesis we checked the reconstruction performance for π^0, η and ω mesons in FoCal detector. We successfully reconstructed all three mesons and extracted signal by subtracting the rotation background which we generated, and found acceptance and efficiency for all three mesons.

We also looked into the raw and corrected yields for π^0 and η meson and found the $\frac{\eta}{pi^0}$ ratio for generated and corrected reconstructed yield for the full Focal psuedorapidity coverage in pp collisions.

4.0.2 Outlook

Future studies can include the above three mesons reconstruction in pPb systems and look into the ratio of their yields and compare the two pp and pPb systems in that regard.

Chapter 5

Supplement figures

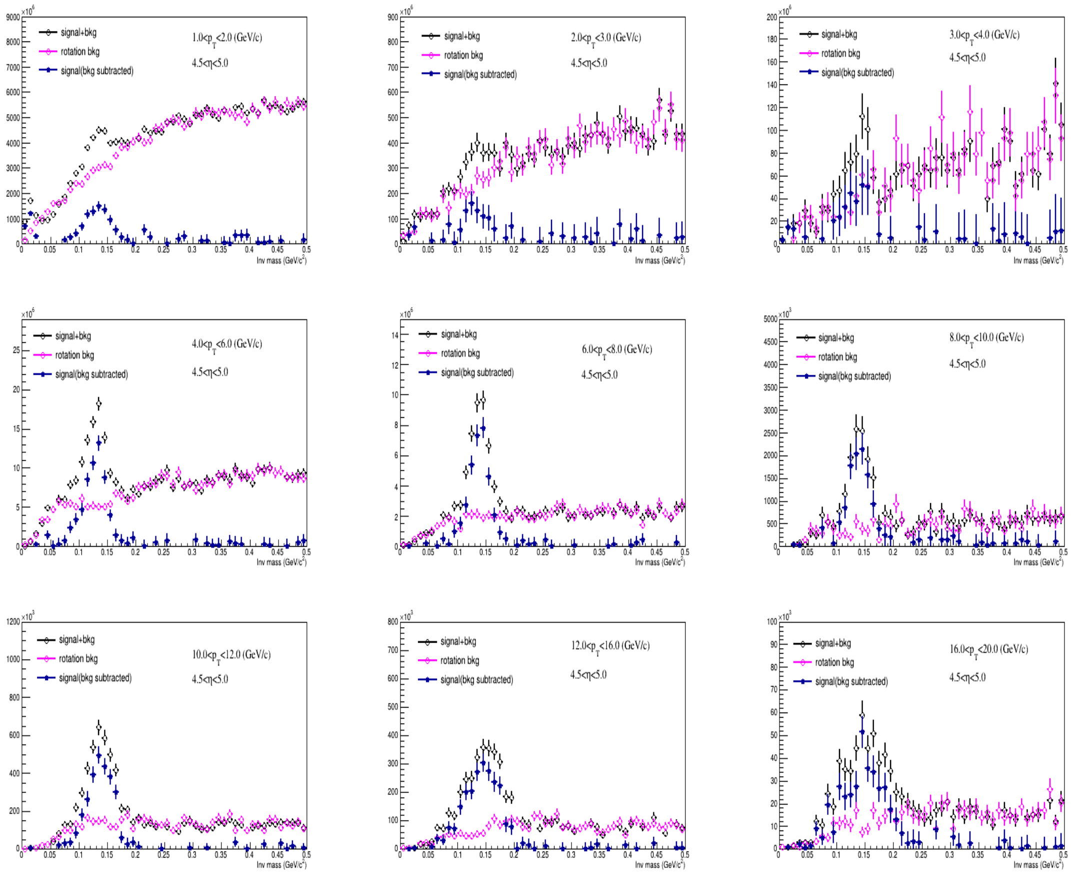

FIGURE 5.1: Invariant mass distribution for π^0 for $4.5 < \eta < 5.0$

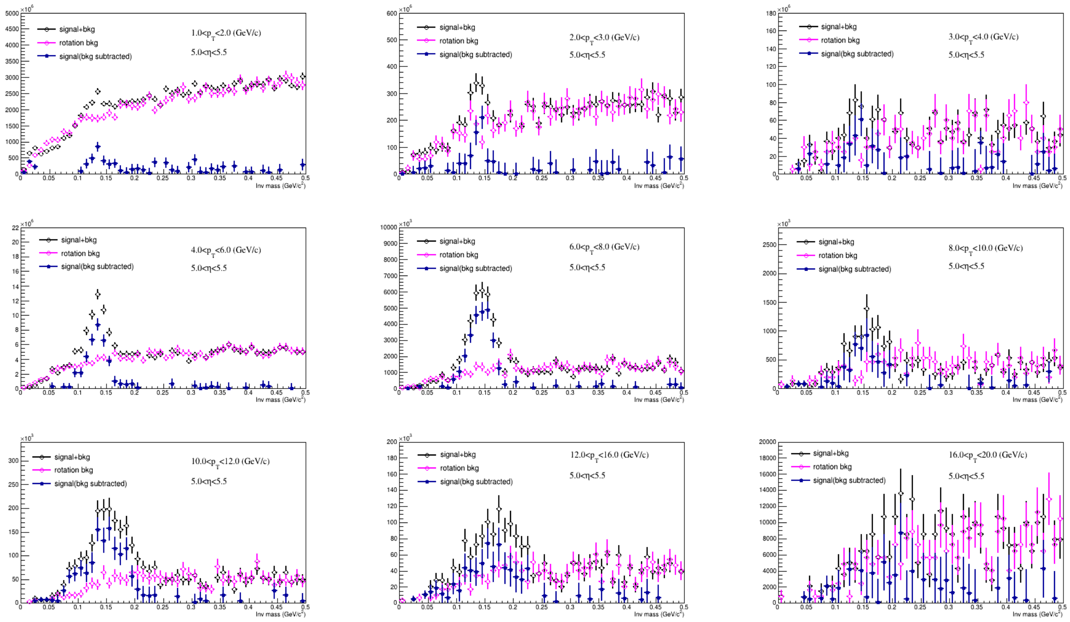

FIGURE 5.2: Invariant mass distribution for π^0 for $5.0 < \eta < 5.5$

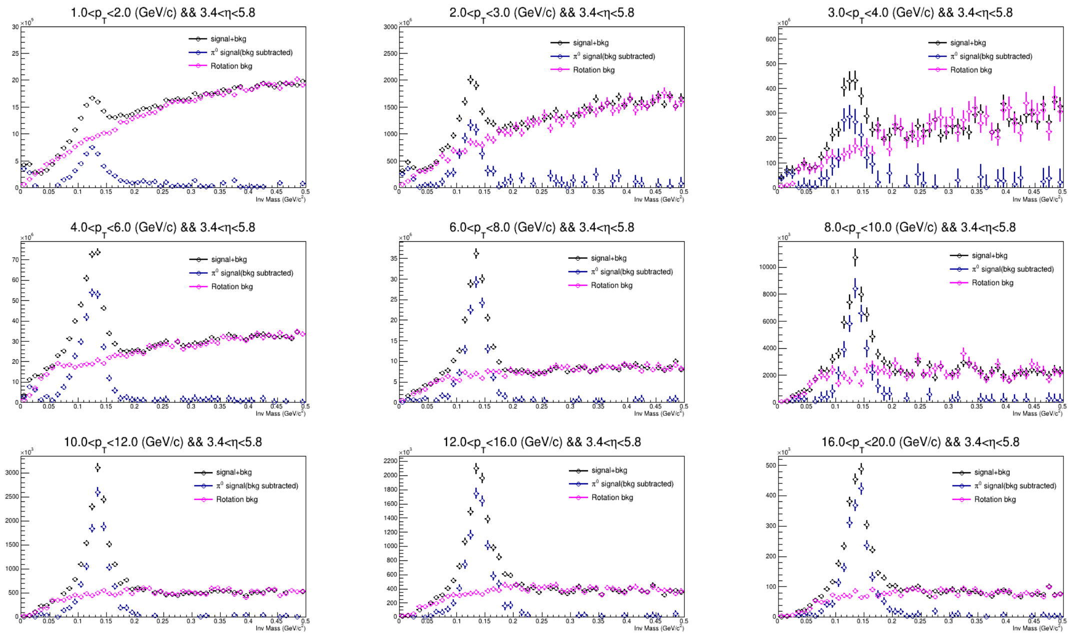

FIGURE 5.3: Invariant mass distribution for π^0 for $3.4 < \eta < 5.8$

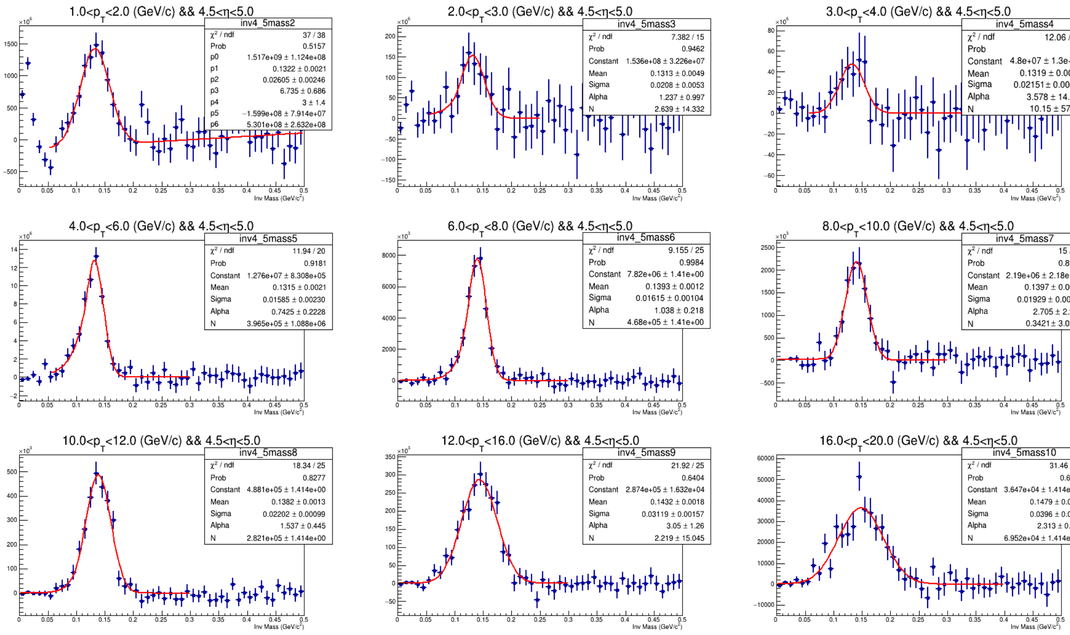

FIGURE 5.4: Fitted invariant mass distribution for π^0 for $4.5 < \eta < 5.0$

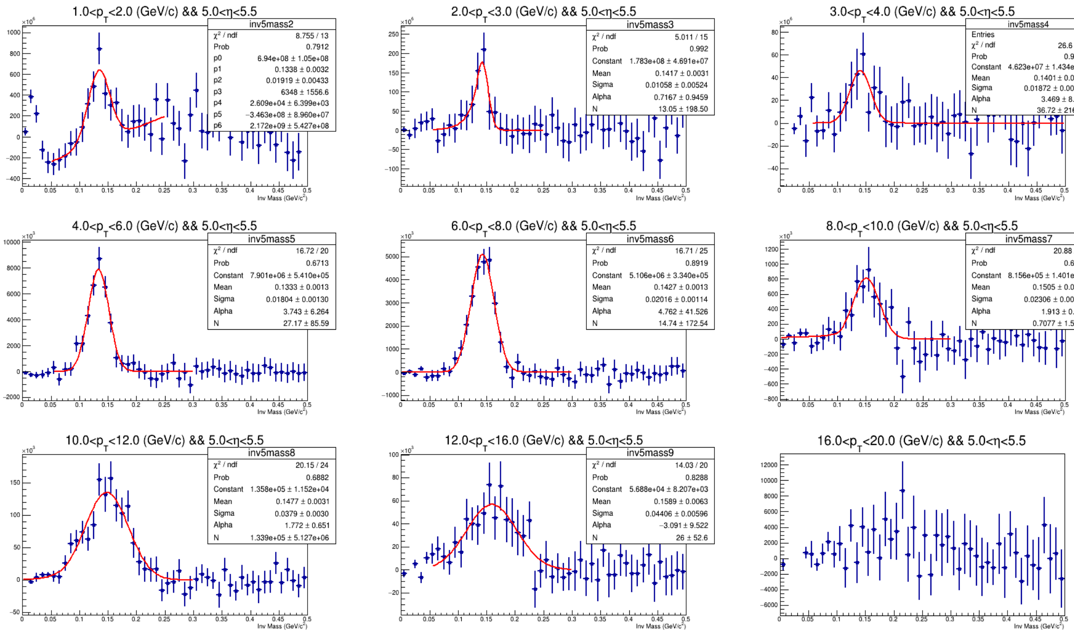

FIGURE 5.5: Fitted invariant mass distribution for π^0 for $5.0 < \eta < 5.5$

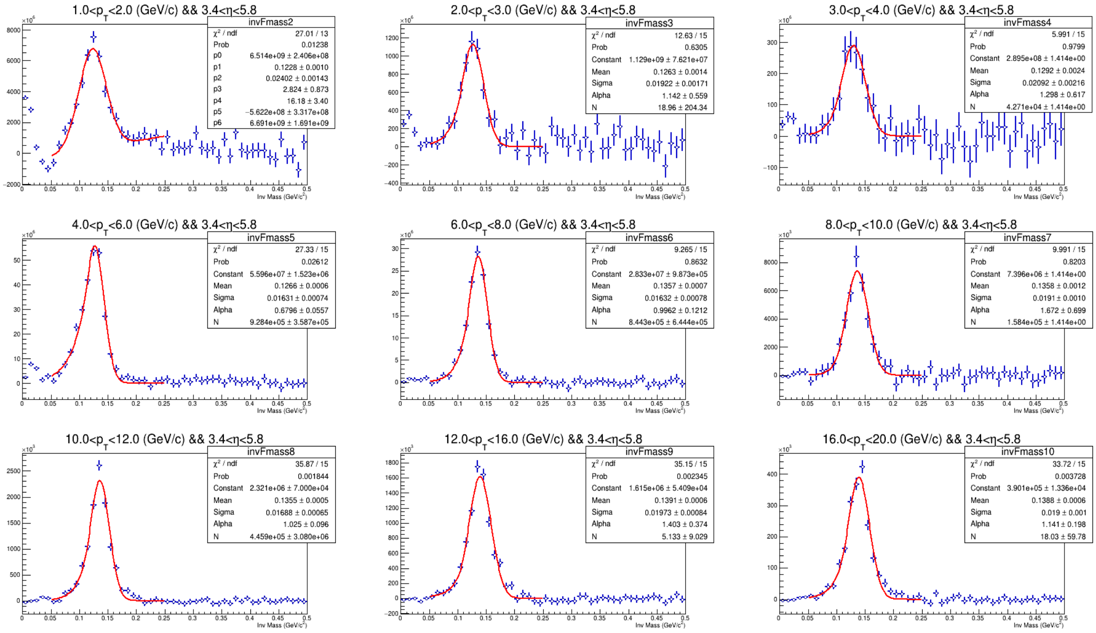

FIGURE 5.6: Fitted invariant mass distribution for π^0 for $3.4 < \eta < 5.8$

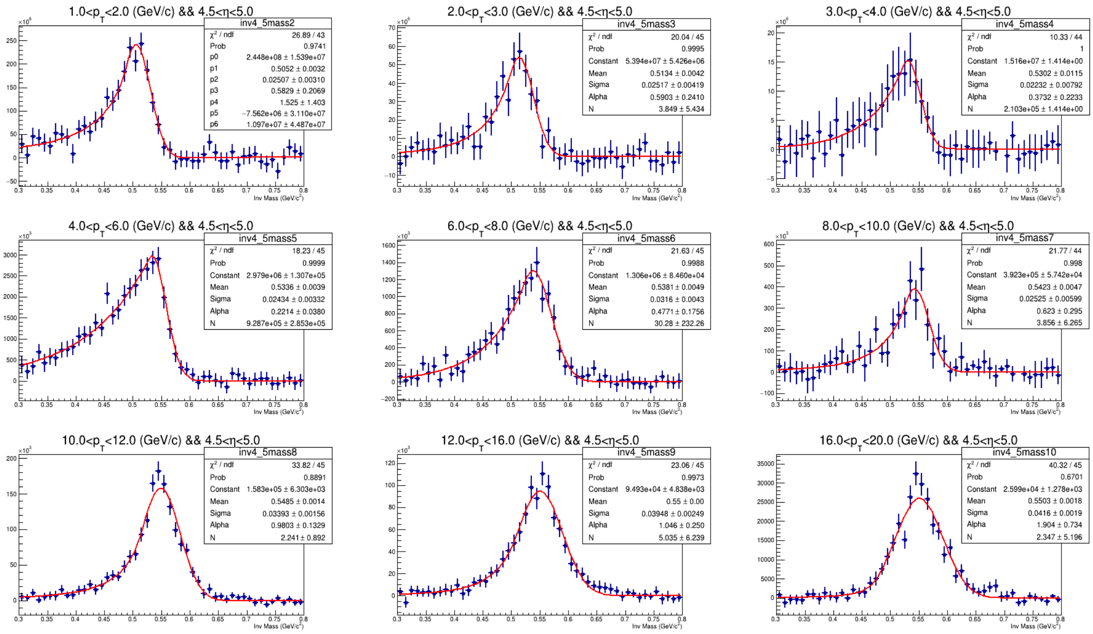

FIGURE 5.7: Fitted invariant mass distribution for η for $4.5 < \eta < 5.0$

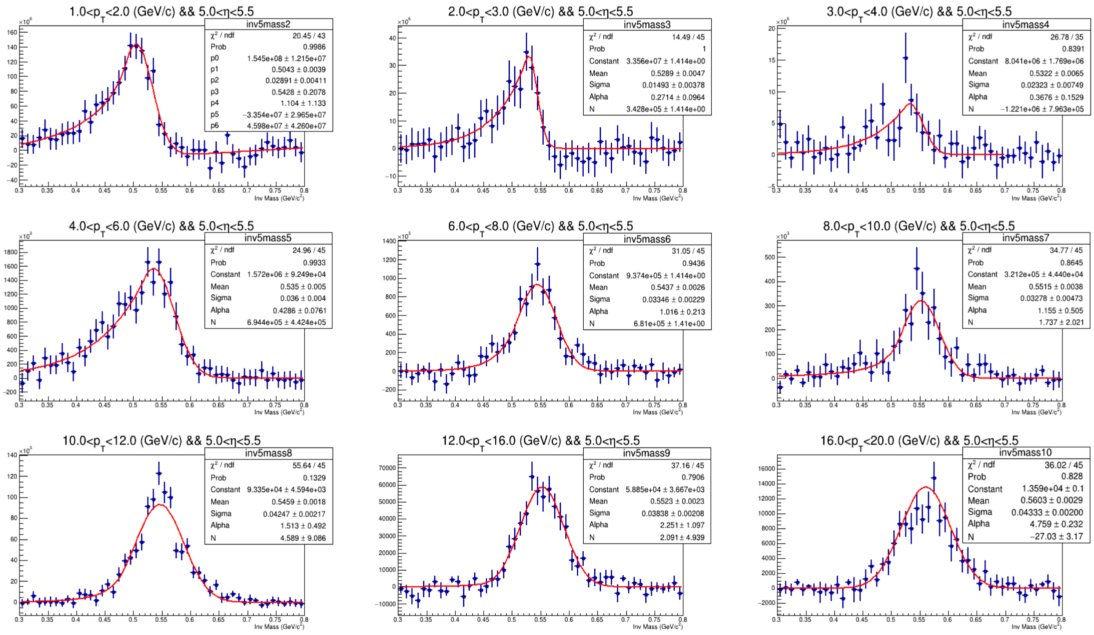

FIGURE 5.8: Fitted invariant mass distribution for η for $5.0 < \eta < 5.5$

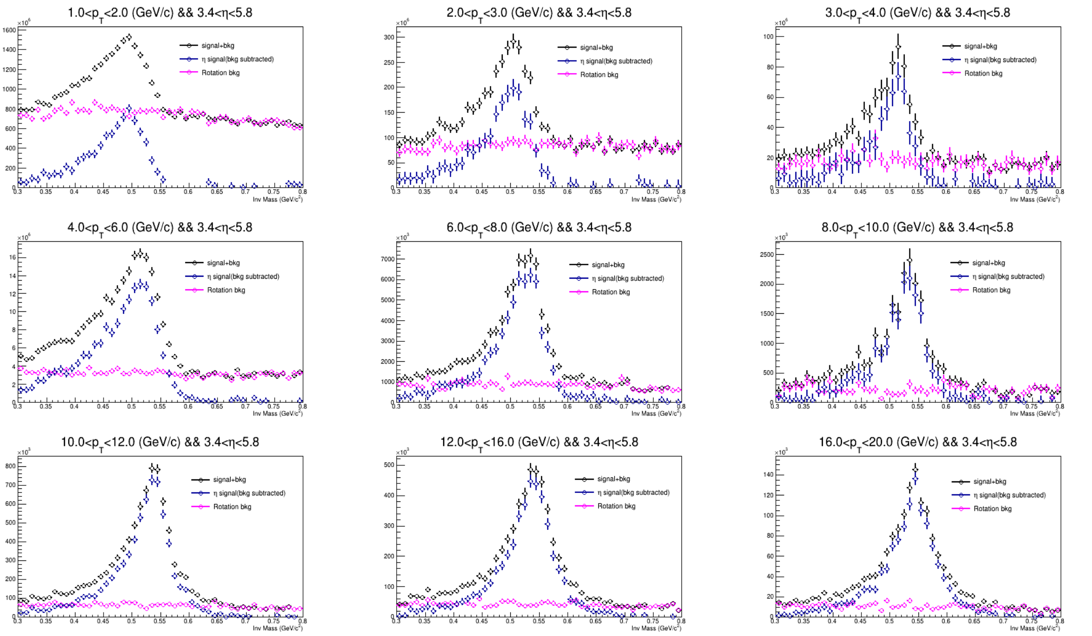

FIGURE 5.9: Invariant mass distribution for η for $3.4 < \eta < 5.8$

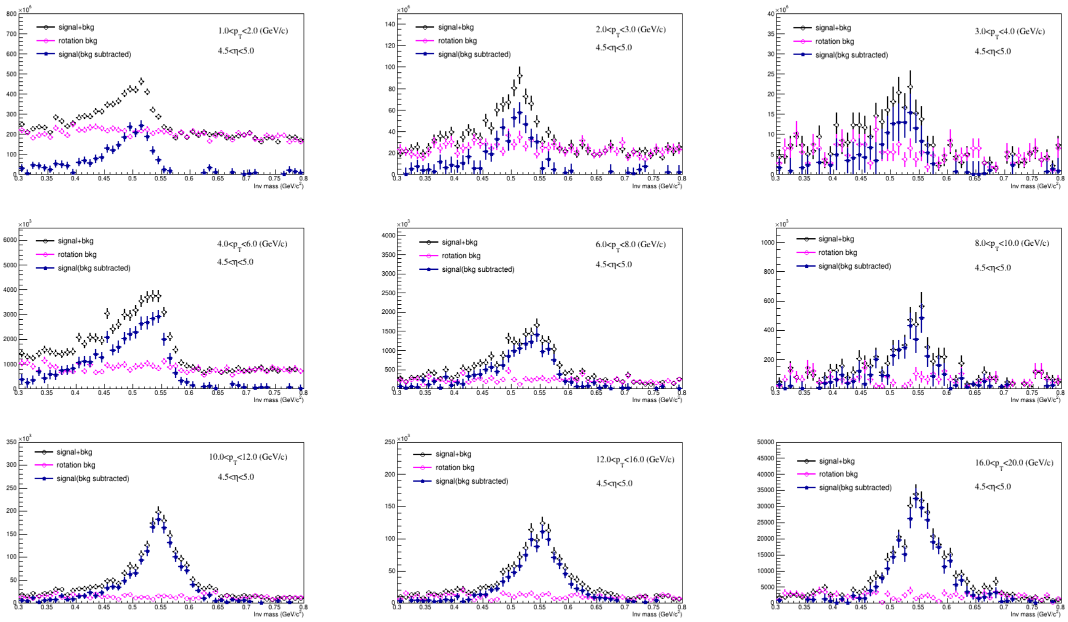

FIGURE 5.10: Invariant mass distribution for η for $4.5 < \eta < 5.0$

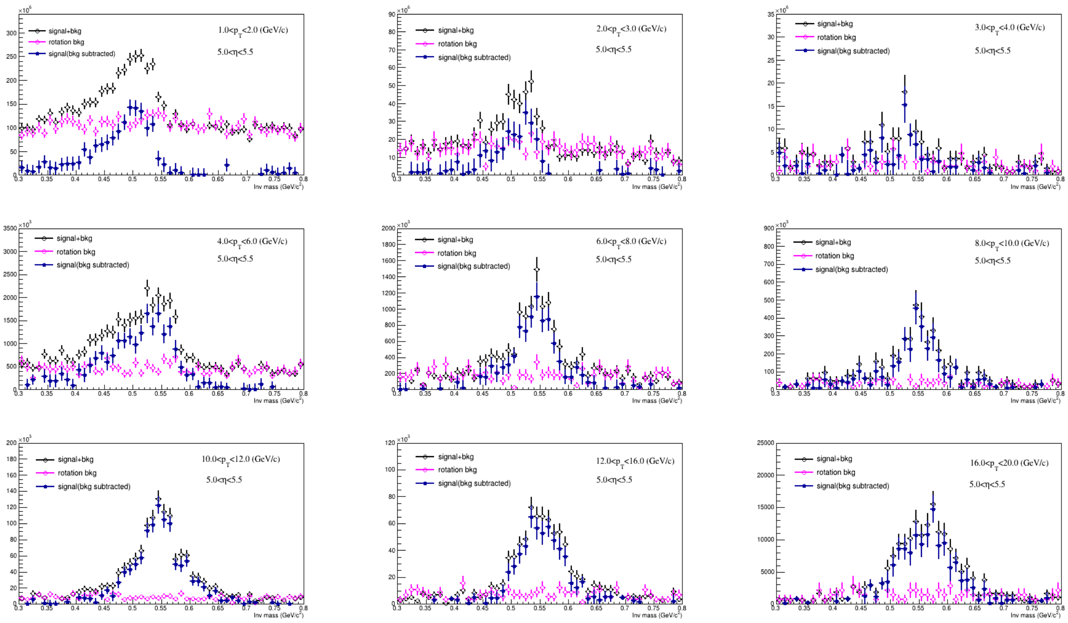

FIGURE 5.11: Invariant mass distribution for η for $5.0 < \eta < 5.5$

Bibliography

[1] Letter of Intent for A Large Ion Collider Experiment [ALICE]. Technical report, CERN, Geneva, 1993.

[2] CERN ALICE Collaboration. Letter of Intent: A Forward Calorimeter (FoCal) in the ALICE experiment. Technical report, CERN, Geneva, 2020.

[3] R Brun, F Bruyant, M Maire, A C McPherson, and P Zanarini. *GEANT 3: user's guide Geant 3.10, Geant 3.11; rev. version.* CERN, Geneva, 1987.

[4] Miklos Gyulassy. The qgp discovered at rhic, 2004.

[5] Miklos Gyulassy and Xin-Nian Wang. HIJING 1.0: A monte carlo program for parton and particle production in high energy hadronic and nuclear collisions. *Computer Physics Communications*, 83(2-3):307–331, dec 1994.

[6] Phillip James Edwin Peebles. Discovery of the hot big bang: What happened in 1948. *The European Physical Journal H*, 39(2):205–223, apr 2014.

[7] Torbjörn Sjöstrand. The pythia event generator: Past, present and future. *Computer Physics Communications*, 246:106910, jan 2020.